The authors answered some of my questions, but I am not satisfied with the answers regarding the method and the conclusions that how the authors calculated the contributions to CCN concentration from BSOA from an ambient dataset. The logic behind it as I see is the involving of BSOA into organic aerosols will change the hygroscopicity parameter κ, then influence the critical diameter of particles that are able to activate, for instance, not 70 nm anymore, which thus change the potential CCN concentration. However, the calculation method from the authors are all based on fixing the size of CCN activation. Then these two things are actually in conflict with each other. Without any CCN measurements with BSOA and without BSOA in your aerosol population, it is hardly to derive the contribution of BSOA to CCN concentration. Your current claims are wrong from your calculations. I strongly suggest the authors change the whole section regarding this part and make proper conclusions with respect to CCN contributions from BSOA.

We appreciate the reviewer's comment. Considering the comment, we calculated d_{act} values at 0.4 % SS for respective 2 h time bins of day using the reconstructed hygroscopicity parameter values of aerosol particles ($\kappa_{t,reconst,org}$ and $\kappa_{t,reconst,BSOA}$ in Text S11), following the method using κ-Köhler theory in Deng et al. (2018). We then used the d_{act} values for the estimate of the fractional contribution of OA/BSOA to CCN number concentrations. Related changes in the manuscript and its SI are as follows.

Texts S12 and S13: They have been deleted because the use of the fixed d_{act} value of 70 nm does not need to be justified anymore.

Figs. 6 and 7 and Tables S9 and S12: Values based on new d_{act} have been applied. Note that all the changes of these values are within −2.22%–1.56% except those associated with BSOA during 0400–0800 JST when the volume fraction of BSOA was low (Fig. S18).

First paragraph of Sect. 4.4: The sentence "In two previous observations at the same site, the average CCN activation diameters of aerosols under 0.41 and 0.42 % SS were 71 and 68 nm, respectively (Kawana et al., 2017; Deng et al., 2018). Based on these facts, all the particles with d_{dry} greater than 70 nm were assumed to be CCN active." has been changed to "The CCN activation diameters (d_{act}) for respective 2 h time bins of day at 0.4 % SS were calculated from reconstructed hygroscopicity parameter values of aerosol particles based on κ-Köhler theory (Text S11)." The

sentence “The diurnal variation of the CCN activation diameter was not considered for the estimate of $F_{CCN,OA}$ and $F_{CCN,BSOA}$ (Text S12).” has been omitted. The phrase “(Text S11)” has been omitted (line 16), and the expression “CCN activation diameter (70 nm)” has been changed to “d_{act}” (line 20).

Last paragraph of Sect. 4.4: The sentences “Furthermore, because fresh BSOA probably become aged after atmospheric transport, the influence of the aging of the estimated fresh BSOA (assuming κ_{BSOA} was as large as that of κ_{ROA} (Table S11)) on $F_{CCN,BSOA}$ was also evaluated. Here, the estimation of $F_{CCN,BSOA}$ in the aged condition ignored the possible change in the CCN activation diameter accompanying the aging processes (Text S13). The possible change in the aerosol size distribution accompanying the aging process was also not considered here.” have been changed to “Furthermore, because fresh BSOA probably become aged after atmospheric transport, the influence of the aging of the estimated fresh BSOA (assuming κ_{BSOA} for the calculation of d_{act} and $F_{CCN,BSOA}$ was as large as that of κ_{ROA} (Table S11)) on $F_{CCN,BSOA}$ was also evaluated. Here, the estimation of $F_{CCN,BSOA}$ in the aged condition ignored the possible change in the aerosol size distribution accompanying the aging process.”

Text S11: The sentence “For the estimate, the observed aerosol particles were assumed to be internally mixed, and all the particles with d_{dry} larger than 70 nm were assumed to be CCN active.” has been changed to “For the estimate, the observed aerosol particles were assumed to be internally mixed, and the CCN activation diameters (d_{act}) under the condition of 0.4 % SS were derived using the reconstructed hygroscopicity parameters ($\kappa_{t,reconst,org}$ and $\kappa_{t,reconst,BSOA}$ for the analysis of the contributions of OA and BSOA, respectively). For the calculation of d_{act}, κ-Köhler theory was applied in the manner of Deng et al. (2018).” Because d_{act} at 0.4 % SS is used now, the hygroscopicity parameter values of inorganic salts presented in Text S11 have also been modified.

Other related changes: All of them are associated with the changes of the values in Figs. 6 and 7 and are presented in the track-change mode version of the manuscript. They are mainly in Sects. 4.4 and 5, and the abstract.

Besides, the expression “(volume concentration less than 0.01×10^{-6} cm^3 m^{-3}; Fig. S18)” in the caption of Fig. 7 has been modified to “(volume concentration less than 0.01 ×

10^{-6} cm^3 m^{-3})", because Fig. S18 does not present volume concentrations but present volume fractions.

We would like to note that the analysis of the contributions of OA and BSOA to CCN concentrations in Sect. 4.4 is not a "sensitivity" analysis to quantify the increase in CCN number concentrations by the presence of OA, as compared to the hypothetical case that OA was absent. In this type of sensitivity analysis, "fractional" contributions of OA and inorganics cannot be quantified because the sensitivity of CCN number concentrations on the presence/absence of OA and inorganics are not additive. In the present study, we quantified fractional contributions of OA and BSOA to CCN number concentrations from the viewpoint of their contributions to the water uptake (amount of water retained) by the aerosol.

Diurnal variation and size-dependence of the hygroscopicity of organic aerosol at a forest site in Wakayama, Japan: their relationship to CCN concentrations

Yange Deng[1], Hikari Yai[1], Hiroaki Fujinari[1], Kaori Kawana[2,3], Tomoki Nakayama[4,5], and Michihiro Mochida[1,4]

[1]Graduate School of Environmental Studies, Nagoya University, Nagoya, Japan
[2]Institute of Low Temperature Science, Hokkaido University, Hokkaido, Japan
[3]Now at Research and Development Center for Global Change, Japan Agency for Marine-Earth Science and Technology, Yokohama, Japan
[4]Institute for Space-Earth Environmental Research, Nagoya University, Nagoya, Japan
[5]Now at Graduate School of Fisheries and Environmental Sciences, Nagasaki University, Nagasaki, Japan

Correspondence to: Michihiro Mochida (mochida@isee.nagoya-u.ac.jp)

Abstract. Formation of biogenic secondary organic aerosol (BSOA) and its subsequent evolution can modify the hygroscopicity of the organic aerosol component (OA) in the forest atmosphere, and affect the concentrations of cloud condensation nuclei (CCN) there. In this study, size-resolved aerosol hygroscopic growth at 85 % relative humidity and size-resolved aerosol composition were measured using a hygroscopic tandem differential mobility analyzer and an aerosol mass spectrometer, respectively, at a forest site in Wakayama, Japan, in August and September 2015. The hygroscopicity parameter of OA (κ_{org}) presented daily minima in the afternoon hours, and it also showed increase with the increase of particle dry diameter. The magnitudes of the diurnal variations of κ_{org} for particles with dry diameters of 100 and 300 nm were on average 0.091 and 0.096, respectively, and the difference of κ_{org} between particles with dry diameters of 100 and 300 nm was on average 0.056. The relative contributions of the estimated fresh BSOA and regional OA to total OA could explain 40 % of the observed diurnal variations and size-dependence of κ_{org}. The hygroscopicity parameter of fresh BSOA was estimated to range from 0.089 to 0.12 for particles with dry diameters from 100 to 300 nm. Compared with the use of time- and size-resolved κ_{org}, the use of time- and size-averaged κ_{org} leads to under- and over-estimation of the fractional contribution of OA to CCN number concentrations in the range from −5.0 to 26 %. This indicates that the diurnal variations and size-dependence of κ_{org} strongly affect the overall contribution of OA to CCN concentrations. The fractional contribution of fresh BSOA to CCN number

Deleted: 4.9

concentrations could reach 0.28 during the period of intensive BSOA formation. The aging of the fresh BSOA, if it occurs, increases the estimated contribution of BSOA to CCN number concentrations by 52–84 %.

Deleted: 50

1 Introduction

The hygroscopicity (ability to absorb water) of organic aerosol (OA) components is governed by their chemical composition, and has two important roles in the atmosphere. It influences light scattering by aerosols (Titos et al., 2016) and affects the ability of aerosols to work as cloud condensation nuclei (CCN; McFiggans et al., 2006). The hygroscopicity of OA may also influence the aqueous chemistry in aerosols and cloud droplets, which provide a potentially important pathway for the formation of secondary organic aerosols (SOA; McNeill, 2015). Nevertheless, the hygroscopicity of OA is not well characterized in terms of its temporal and spatial variations, size-dependence, and its relationship with the chemical composition of OA, given that OA is a complex mixture of a number of compounds.

Studies on the hygroscopicity parameter κ of OA (κ_{org}; Petters and Kreidenweis, 2007) in different locations have presented different characteristics of temporal variation and size-dependence. Based on a year-long observation under supersaturated water vapor conditions (SUPS) at a downwind site of Manaus in central Amazonia, Thalman et al. (2017) reported that κ_{org} presented the lowest value of ~0.1 in September and the highest value of ~0.15 in December, and that the ranges of the diurnal variations of κ_{org} were 0.10 to 0.16 (night to day) and 0.08 to 0.14 (night to day) under the influence of local biomass-burning air masses during the dry season and urban-pollution air masses during the wet season, respectively. Bougiatioti et al. (2016) reported diurnal variation of κ_{org} in the range 0.09–0.18 (day to night) under SUPS for particles influenced by biomass burning in the eastern Mediterranean. Deng et al. (2018) reported diurnal variation ranges of κ_{org} of 0.09 to 0.30 (day to night) and 0.16 to 0.24 (day to night) on days with and without evident new particle formation (NPF), respectively, under SUPS (0.23 % water vapor supersaturation (SS) condition) in a forest in Wakayama, Japan. Different from the above studies, at a rural site in the southeastern United States, a small diurnal variation of κ_{org} (~0.13 to ~0.17, night to day) under SUPS was observed (Cerully et al., 2015). With respect to the size-dependence of κ_{org}, airborne studies over United States, Canada, Pacific Ocean, and the Gulf of Mexico for a variety of air mass types, presented a decrease of κ_{org} (from 0.13 to 0.06) with increase of the particle modal diameter (from 130 to ~210 nm) under subsaturated water vapor conditions (SUBS) (Shingler et al., 2016). By contrast,

ground-based observations in the City of Nagoya in Japan under SUBS presented relatively low κ_{org} in small particles (0.12–0.15; 60 and 100 nm) and high κ_{org} in large particles (0.17–0.22; 200 and 359 nm) (Kawana et al., 2016). For aerosols in forest areas, whereas Deng et al. (2018) reported a difference of 0.03 in mean κ_{org} between sub-100 nm particles (κ_{org} was 0.19) and ~150 nm particles (κ_{org} was 0.22), Thalman et al. (2017) did not identify any size-dependence of κ_{org} for 94–171 nm particles. The hygroscopicity of laboratory-generated model SOA was also reported to be size-dependent. Frosch et al. (2011) reported that the κ of α–pinene SOA at SUPS at 100 nm (~0.12) was ~0.06 higher than at 200 nm. Zhao et al. (2015) reported that the κ of model SOA at SUPS produced by different precursors at 50, 100, and 200 nm were ~0.17, ~0.11, and ~0.07, respectively. Tritscher et al. (2011) also found that small (50 nm) α-pinene SOA particles had a higher κ than large ones (150 nm) at SUBS, although the difference was small (0.03). Frosch et al. (2013) reported that the κ of β-caryophyllene SOA decreased with increase of SS, which can be interpreted as the increase of κ with the increase of particle diameter, and that the maximum of the difference was about 0.1.

The variations in κ_{org} observed in the aforementioned studies may have great influence on the prediction of CCN. Based on global climate modelling simulations, Liu and Wang (2010) reported that CCN concentration would change within 40 % by changing the κ of SOA by ±50 % (from 0.14 to 0.07 or 0.21). Rastak et al. (2017) reported that the difference of the aerosol radiative effects between κ_{org} of 0.05 and 0.15 was −1.02 W m^{-2}, the order of which is the same as that of the overall climate forcing effect of anthropogenic aerosol during the industrial period. Based on CCN closure studies, Wang et al. (2008) reported that, for above-cloud aerosols with high volume fractions of OA, while the CCN number concentration closure could be achieved using κ_{org} of 0.12, the use of κ_{org} of 0.25 led to overestimation of the CCN number concentration by 50 %. Mei et al. (2013b) reported that the increase of κ_{org} from 0.08 to 0.13 led to 30 % increase of the calculated CCN number concentration and that increase from 0.03 to 0.18 doubled the concentration. It is therefore important to study the temporal variation and size-dependence of κ_{org} in more locations where OA dominates the aerosol chemical composition, to characterize the κ_{org} values and to represent the κ_{org} appropriately in model predictions of CCN number concentrations.

The temporal variation and size-dependence of κ_{org} of ambient aerosol is reported to relate with variations in the chemical composition of OA, which can result from the mixing of aerosols of different origins, formation of SOA, and aging processes (Cerully et al., 2015; Bougiatioti et al., 2016; Shingler et al., 2016; Thalman et al., 2017; Deng et al., 2018). The size-dependent chemical composition of model SOA has been explained by the size-dependent contributions of different organic vapors to particle growth (e.g., Winkler et al., 2012; Ehn et al., 2014; Zhao et al., 2015; Zhao et al., 2016). The size-dependent κ of model SOA has also been explained from the viewpoint of size-dependent chemical composition (Zhao et al., 2015; Frosch et al., 2013) and other factors: the dependence of water activity on particle size, the dependence of the surface tension on the solution concentration, and the evaporation of semi-volatile SOA under high SS conditions (Frosch et al., 2011; Frosch et al., 2013; Zhao et al., 2015). In recent studies, the variation of κ_{org} was explained by the variation of OA subcomponents derived from positive matrix factorization (PMF) analysis of OA mass spectra (Cerully et al., 2015; Bougiatioti et al., 2016). From these studies it is reported that the daily variation of κ_{org} could be well explained by the daily variation in the contributions of the retrieved PMF factors to κ_{org}.

In the forest atmosphere, the oxidation of biogenic volatile organic compounds (BVOC) emitted by vegetation can produce substantial amounts of biogenic secondary organic aerosols (BSOA; Tunved et al., 2006; Pöschl et al., 2010; Han et al., 2014). BSOA is reported to contribute to the growth of newly formed particles in forests (e.g., Han et al., 2013; Yu et al., 2014; Zhou et al., 2015). BSOA may also condense on preexisting background particles or particles transported with inflowing air masses (e.g., Cerully et al., 2015; Thalman et al., 2017). Moreover, BSOA is subject to aging processes that include photochemical oxidation and aqueous phase reactions that must depend on ambient meteorological conditions (e.g., Han et al., 2014; Thalman et al., 2017). Such processes could result in time- and size-dependent variation in the chemical composition of OA and thus time- and size-dependent κ_{org} in the forest atmosphere. However, the characteristics of the temporal variations and size-dependence of κ_{org}, and their relationships to the atmospheric processes of BSOA in forest environments, are not well understood.

We performed field observation at a forest site in Wakayama, Japan in August and September, 2015, and characterized the diurnal variations and size-dependence of κ_{org}. The variations and dependence were interpreted based upon the size-resolved

chemical composition of OA from the viewpoint of BSOA formation. Furthermore, the influence of these variations on the fractional contribution of OA and BSOA to the CCN concentration was assessed. Previous observational studies at the site indicated that BSOA formation was intensive and that aging occurred after formation (Han et al., 2014; Deng et al., 2018). It was also observed that κ_{org} was time and size dependent and that the contribution of OA and BSOA to CCN number concentrations could be substantial (Deng et al., 2018). This work is an extension of previous studies on the hygroscopicity and CCN activity of aerosols, and the contributions of OA and BSOA to the CCN concentration, in the same forest (Kawana et al., 2017; Deng et al., 2018). It is intended to clarify the diurnal variation and size-dependence of the hygroscopicity of OA and their influence on the contributions of OA and BSOA to CCN.

2 Field observation

The field observation was performed at Wakayama Forest Research Station, Kyoto University (34.06° N, 135.52° E, about 500 m above sea level), located in the central part of the Kii Peninsula. The observation site is about 70 km south of Osaka (2.7 million inhabitants) and 60 km northwest of the North Pacific. Both coniferous trees (such as *Cryptomeria japonica*, *Chamaecyparis obtuse*, and *Pinus densiflora*) and broad-leaf trees (such as *Quercus serrata* and *Quercus crispula*) are distributed on the Kii Peninsula (Okumura, 2009). The study period was from 1430 Japan Standard Time (JST) on 31 August to 0600 JST on 22 September 2015.

The hygroscopic growth at 85 % relative humidity (RH), number-size distributions, and size-resolved chemical composition of ambient aerosols were measured using a hygroscopicity tandem differential mobility analyzer (HTDMA), a scanning mobility particle sizer (SMPS), and a high-resolution time-of-flight aerosol mass spectrometer (AMS), respectively. Ambient air was aspirated from an inlet about 7.5 m above the ground. The air was transferred through a $PM_{2.5}$ cyclone (URG) installed at the lower end of the 10.4 m stainless-steel inlet tubing (1/2-inch OD) and introduced to the instrument room at a flow rate of 16.7 L min^{-1}. A manifold combined with an assistant pump (ULVAC, DA30S) was used to split the air flow, and the sample flow for the instrument system composed of the HTDMA, SMPS, and AMS was 0.9 L min^{-1}. The sample flow upstream of the AMS was dried with two diffusion driers containing silica gel. The sample flow to the HTDMA and SMPS was dried with three diffusion driers, in series, two with silica gel and one with molecular sieves.

In the HTDMA, the dried aerosol (RH < 1.8 %) was passed through the first differential mobility analyzer (DMA1; 3081, TSI), where the aerosol was classified, and quasi-monodisperse particles of 30, 50, 70, 100, 200, 300, and 360 nm in diameter (d_{dry}) were obtained. The setting for the classification was fixed for 5 min at each diameter. In each hour, the sequential diameter setting of DMA1 was 30, 50, 70, 100, 200, 360, 30, 50, 100, 200, 300, and 360 nm. During 0550–0554 JST and 1750–1754 JST, the setting of DMA1 was for system performance check. The classified aerosol was passed through a Nafion humidifier (MD-110-24S-4, Perma Pure) where it was humidified to ~85% RH. The aerosol was then introduced to a second DMA (DMA2; 3081, TSI) coupled to a condensation particle counter (CPC, 3775, TSI), which was operated by scanning the voltage of DMA2. For both DMA1 and DMA2, the aerosol flow rate was 0.3 L min^{-1} and the sheath-to-sample flow ratio was 10:1. The residence time of the monodisperse particles from the outlet of the humidifier to the inlet of DMA2, where the RH was considered to be ~85 %, was approximately 11 s. The sheath air flow of DMA2 was also humidified using another Nafion humidifier (PD-100T-12MSS, Perma Pure). The RH (temperature) measured (HMP237, Vaisala) at the inlets of aerosol flow and sheath flow to DMA2 were 85.0 ± 0.2 % (20.3 ± 0.5 ℃) and 85.0 ± 0.2 % (20.4 ± 0.5 ℃), respectively, and that at the outlet of the sheath flow of DMA2 was 86.0 ± 0.3 % (20.3 ± 0.6 ℃). For analysis of the particle hygroscopic growth, RH of 85 % was applied. The SMPS for the measurement of aerosol number-size distributions was composed of a third DMA (DMA3; 3080, 3081, TSI) and a CPC 3772 (TSI). The aerosol flow (RH < 1.6 %) was 0.3 L min^{-1} and the sheath to aerosol flow ratio was 10:1. At the inlet of CPC 3772, the sample flow was diluted to 1 L min^{-1} with purified dry air, which was generated using a compressor (RD-45-N, IAC) and an air dryer (QD 30-50, IAC). The aerosol number-size distributions were measured for a dry diameter range of 13.8–749.9 nm every 5 min. The performances of the three DMAs were assessed using standard size PSL particles before and after the observation (Text S1). Furthermore, an aqueous solution of ammonium sulfate (AS) (99.999 % purity, Sigma-Aldrich) was nebulized and the generated aerosols were dried and introduced to the HTDMA, to assess the consistency of the sizing of the two DMAs under dry condition, and to validate the RH setting before the observation (Text S2). The setup and calibration procedures of the AMS were the same as those for the observations in 2014 (Deng et al., 2018). The V-mode (MS and PToF modes) data was analyzed using the Igor high resolution data analysis package (PIKA1.20Q, Igor 6.37) to obtain the bulk and size-resolved mass concentrations of the chemical components (sulfate (SO_4), ammonium (NH_4), nitrate (NO_3), chloride (Chl), and OA), and the atomic ratios of O to C (O:C ratio) and H to C (H:C ratio) for organics. In

addition, high-resolution bulk OA mass spectra observed in V-mode were subjected to PMF analysis (Paatero and Tapper, 1994; Ulbrich et al., 2009) (Sect. 3.3, Text S3). The RH of the sample flow was lower than 0.5 %.

A single wavelength particle soot absorption photometer (1λ-PSAP, 567 nm, Radiance Research Inc.) with a thermodenuder maintained at 300 °C, was deployed to obtain the mass concentration of sub-micrometer black carbon (BC; Kondo et al. 2009; Deng et al., 2018). The mixing ratios of target gaseous species, NO-NO_2-NO_x, CO, CO_2, and O_3, were monitored using commercial instruments (APNA-370, Horiba for NO-NO_2-NO_x; model 48ij, Thermo Fisher Scientific for CO; LI-820, LI-COR for CO_2; model 49ij, Thermo Fisher Scientific for O_3). Meteorological data were collected (Kyoto University, 2017). Air temperature, RH (HMP-155, Vaisala), precipitation (RH-5E, IKEDA-KEIKI), and solar radiation (CMP3-L, Campbell) were used in this study.

All the observation data except meteorological data were screened to eliminate data that might have been under the strong influence of local anthropogenic emissions, for example, from vehicles. This was performed by omitting data with spikes in the number concentrations of aerosols from their size distribution data, and in the mass concentration of BC (Text S4).

3 Data analysis

3.1 Hygroscopicity of ambient aerosols

The hygroscopic growth factor of aerosol particles, g_f, was defined as the ratio of the particle wet diameter (d_{wet}, 85 % RH) to the corresponding dry diameter (d_{dry}). The distributions of g_f for specific d_{dry} ($n(g_f)$, i.e., the number distribution of particles as a function of g_f) were retrieved using the Twomey algorithm as presented by Mochida et al. (2010) with consideration of the shape of the transfer functions of the two DMAs. The difference in the processing is that the transfer function and the $n(g_f)$ in this study were analyzed and presented in the fine mode of 1024 diameter bins per decade while 64 bins per decade were used in Mochida et al. (2010). The g_f probability distribution function, g_f-PDF, is the normalized $n(g_f)$. The g_f-PDF in this study is presented in linear scale, which was converted from the original logarithmic scale distribution. The time-resolved mean value of g_f for respective d_{dry}, $g_{f,m}$, was calculated as follows.

$$g_{f,m} = \frac{\sum n(g_f) g_f}{\sum n(g_f)} \quad (0.8 \le g_f \le 2.2 \text{ for } 30 \le d_{dry} \le 300 \text{ nm, or } 0.8 \le g_f \le 2.0 \text{ for } d_{dry} = 360 \text{ nm}) \quad (1)$$

For ambient particles, time-resolved mean-water-volume equivalent g_f ($g_{f,mw}$, i.e., the average of g_f that corresponds to the mean water volume retained by particles of certain d_{dry}) was also calculated using Eq. (2) (Kawana et al., 2016).

$$g_{f,mw} = \left[\frac{\sum n(g_f)(g_f{}^3-1)}{\sum n(g_f)} + 1\right]^{\frac{1}{3}} \quad (0.8 \le g_f \le 2.2 \text{ for } 30 \le d_{dry} \le 300 \text{ nm, or } 0.8 \le g_f \le 2.0 \text{ for } d_{dry} = 360 \text{ nm}) \tag{2}$$

The hygroscopicity parameter of ambient particles at 85 % RH (κ_t) was calculated following the κ-Köhler theory (Petters and Kreidenweis, 2007).

$$\kappa_t = \left(g_{f,mw}{}^3 - 1\right)\left[\frac{\exp\left(\frac{4\sigma M_w}{RT\rho_w d_{wet}}\right)}{0.85} - 1\right] \tag{3}$$

where σ is the surface tension at the solution/air interface, M_w and ρ_w are the molecular mass and density of pure water, respectively, d_{wet} is the product of $g_{f,mw}$ and d_{dry}, R is the universal gas constant, and T is the temperature in kelvin. In this study, the mean temperature at the inlets of aerosol flow and sheath flow of DMA2, weighted by their flowrates, was applied as T (294 K) and the surface tension of pure water at this temperature (Vargaftik et al., 1983) was used as σ in Eq. (3). Because κ_t was calculated from $g_{f,mw}$, the aerosol mixing state was not considered in the analysis of κ in this study.

3.2 Hygroscopicity of OA

The hygroscopicity parameter of organics, κ_{org}, was calculated using Eq. (4) assuming the volume additivity of water retained by different aerosol components (Petters and Kreidenweis, 2007).

$$\kappa_t = \varepsilon_{org}\kappa_{org} + \varepsilon_{inorgsalt}\kappa_{inorgsalt} + \varepsilon_{BC}\kappa_{BC} = \varepsilon_{org}\kappa_{org} + \sum_{i=1}^{5}\varepsilon_i\kappa_i + \varepsilon_{BC}\kappa_{BC} \tag{4}$$

Here, κ_t is the hygroscopicity parameter of ambient aerosol at 85 % RH calculated using Eq. (3), while κ_{org}, $\kappa_{inorgsalt}$, and κ_{BC} are the hygroscopicity parameters of OA, inorganic salts, and BC, respectively. The volume fractions of OA, inorganic salts, and BC are ε_{org}, $\varepsilon_{inorgsalt}$, and ε_{BC}, respectively, and ε_i and κ_i are the volume fraction and hygroscopicity parameter of the inorganic salts: ammonium nitrate (AN), sulfuric acid (SA), ammonium hydrogen sulfate (AHS), letovicite (LET), and ammonium sulfate (AS). The ε_{org}, ε_i, and ε_{BC} were calculated based on the size-resolved mass concentrations of organics, sulfate, nitrate, and ammonium from the AMS, and the sub-micrometer BC mass concentrations from the PSAP. BC was

assumed to have the same mass-size distribution as OA. The aerosol particles were assumed to be spherical and without voids. PToF mode data in vacuum aerodynamic diameter (d_{va}) ranges that were ~1.0 (0.98–0.99) to 2.0 times that of d_{dry}, corresponding to the particle density of ~1.0 (0.98–0.99) to 2.0 g cm^{-3}, were adopted. More details about the calculations of the size-resolved ε_{org}, ε_i, and ε_{BC} are presented in Text S5. The derivation of κ_i was based on the online Extended AIM Aerosol Thermodynamics Model II (E-AIM II, http://www.aim.env.uea.ac.uk/aim/kohler/input_kohler.html; Clegg et al., 1998; Wexler and Clegg, 2002) as presented in Text S6 and Table S3. The κ of BC was assumed to be zero. Because of the low signal intensity of the PToF data in the sub-100-nm d_{va} range (Text S7), the κ_{org} was only derived for particles with d_{dry} of 100, 200, 300, and 360 nm. Furthermore, to assess the influence of the choice of the d_{va} range on the derivation of κ_{org}, the derived κ_{org} for particles with d_{dry} of 100 nm using the chemical composition in the d_{va} range 98–197 nm, was compared with that using the chemical composition in the d_{va} range 69–138 nm (Fig. S4). The result indicates that κ_{org} was not sensitive to change in the selected d_{va} range when ε_{org} was greater than 40 %. Note that, although the volume additivity assumption between organics and inorganics may not necessarily hold (Vaishya et al., 2013; the κ_{org} derived in the manner in this study represents the perturbation of κ_i as a result of the presence of organics), the inverse linear correlation between κ_i and ε_{org} (correlation coefficients: −0.45 to −0.83; Fig. S5) suggests that the additivity holds well for the aerosols studied.

3.3 PMF analysis of OA mass spectra

To characterize the diurnal variations and size-dependence of κ_{org}, the high-resolution OA bulk mass spectra derived from the V-mode AMS data were subjected to PMF analysis (Text S3), followed by derivation of the size-resolved contributions of the PMF factors to the OA mass concentration (Text S8). A two-factor PMF solution was adopted, which resolved two oxygenated OA factors: one with a lower atomic O:C ratio (0.47) named less-oxygenated organic aerosol (LOOA), and the other with a higher O:C ratio (0.95) named more-oxygenated organic aerosol (MOOA). The low relative residual (2.6 %) for the bulk mass spectra supports the use of the two PMF factors to illustrate the observed OA. Note that the two OA factors resolved here represent two different groups of OA chemical structures, not necessarily two different OA sources (Zhang et al., 2011). The use of a PMF result with more factors could make illustration of the variation of κ_{org} complex and was not adopted. The PToF mode OA mass spectra in 2 h time resolution were attributed to the two PMF factors through multivariable linear regression

(Text S8). For particles with d_{dry} equals to or larger than 100 nm, the variation of κ_{org} was discussed with regard to the variations of the two PMF factors. Furthermore, the hygroscopicity parameters for the two OA fractions were derived, and then used to estimate the hygroscopicity of freshly formed BSOA (Sect. 4.2).

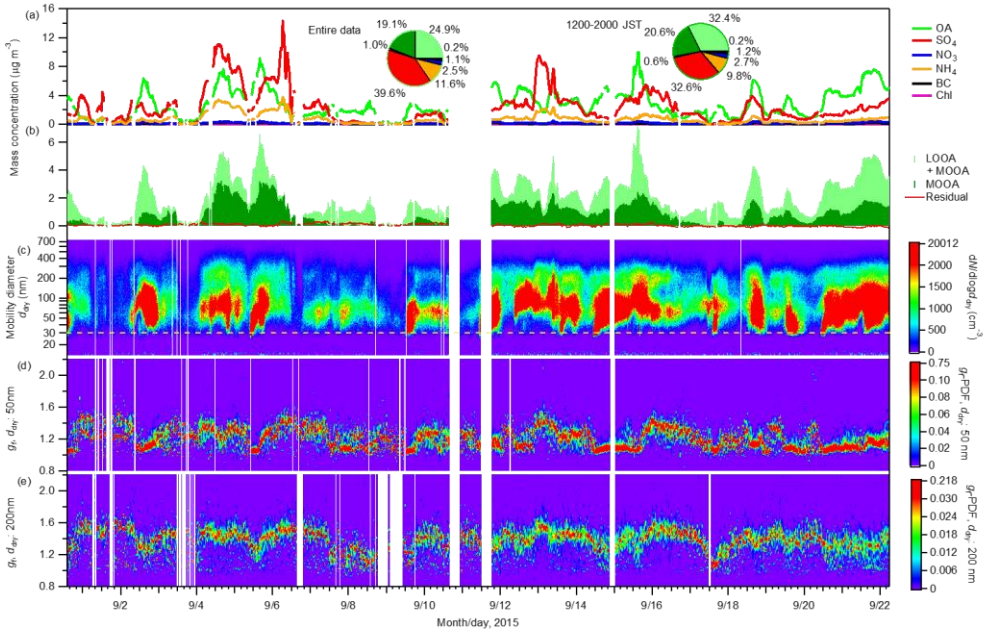

Figure 1: Time series of (a) sub-micrometer mass concentrations of non-refractory aerosol chemical components (OA, SO_4, NO_3, NH_4, and Chl) from the AMS measurement and BC from the PSAP measurement, (b) mass concentrations of LOOA and MOOA, and the residuals from the PMF analysis, (c) aerosol number-size distributions, and g_f-PDF of aerosol particles with d_{dry} of (d) 50 nm and (e) 200 nm. The two pie charts in panel (a) present the mass fractions of chemical components for the entire study period and for the afternoon hours (1200–2000 JST) during the study period. The dashed line in panel (c) represents a diameter of 30 nm.

4 Results and discussions

4.1 Overview of the observations

4.1.1 Meteorological conditions, gaseous species, and aerosol chemical composition

During the measurement period with effective data, the mean ± standard deviation (SD) of the temperature and RH of the ambient air were 18.2 ± 2.4 ℃ and 94.2 ± 7.6 %, respectively. Precipitation events occurred intermittently during 1–3, 6–10, and 16–17 September (Fig. S7). Backward air mass trajectories (Fig. S9) generated using NOAA's HYSPLIT atmospheric transport and dispersion modeling system (Draxler and Hess, 1998) indicate that, except on 1 and 17 September, most of the air masses that arrived at the observation site had traveled from the Japan archipelago (and even from the Asian continent) within five days, and may have transported aged anthropogenic pollutants to the observation site. The mean ± SD of the BC concentration during the entire study period was 0.07 ± 0.06 μg m^{-3} (Fig. S7). The mean ± SD of the mixing ratios of CO, NO, NO_2, NO_x, and O_3 during the entire study period were 164 ± 42, 0.33 ± 0.12, 0.56 ± 0.35, 0.63 ± 0.38, and 11.5 ± 8.4 ppb, respectively (Fig. S7). The concentration of BC was low, and the mixing ratios of CO and NO_x were modest. A daily maximum of BC appeared in the afternoon hours (Fig. 2), which however might have been caused by the charring of OA at the heating temperature of 300 ℃. The mixing ratios of CO and NO_x tended to be relatively high during 1000–2200 JST (Fig. S8), which might have been caused by the transport of anthropogenic pollution to the surface site by enhanced vertical convection in the daytime. The concentration of O_3 was substantial and presented obvious diurnal variation (Fig. S7). On average, O_3 peaked during noon with the solar radiation (Fig. S8), indicating the occurrence of photochemical reactions during the daytime.

The time series of the mass concentrations of aerosol chemical components and aerosol number-size distributions are presented in Fig. 1. Among non-refractory aerosol chemical components derived from the AMS and BC derived from the PSAP (total concentration: 6.2 ± 4.4 μg m^{-3}), organics on average accounted for the largest fraction (45.0 %; of which LOOA and MOOA accounted for 24.9 % and 19.1 %, respectively), followed by sulfate (39.6 %) and ammonium (11.6 %). The contribution of nitrate, BC, and chloride were minor: their mass fractions were on average 2.5 %, 1.1 %, and 0.2 %, respectively. The contribution of OA to the sub-micrometer aerosol mass increased and that of sulfate decreased in the afternoon hours (1200–2000 JST). The mean aerosol number concentration (N_{CN}) was 1241 ± 1012 cm^{-3}. The geometric mean diameter of the aerosols

ranged from 45 to 154 nm with a mean ± SD of 88 ± 17 nm. No strong burst of small particles (i.e., d_{dry} < 30 nm) was identified during the observation, which is different from the two former observations in 2010 and 2014 (Han et al., 2013; Deng et al., 2018).

The diurnal variation of the number-size distributions and the mass concentrations of the chemical components of aerosols are presented in Fig. 2. The N_{CN}, OA, and LOOA presented similar diurnal variation patterns. Their daily minima were observed between 0600 and 0830 JST. After 0830 JST, they increased monotonically and reached their maxima during 1500–1800 JST. Then they gradually decreased until approximately 0600 JST of the next day. MOOA also increased slowly (following the trend of LOOA) in the daytime and reached its maximum around 1800 JST. The pattern of the enhancement of OA in the daytime followed that of the solar radiation (Fig. 2b), indicating that the enhancement of OA was caused by the formation of BSOA through photochemical reactions of BVOC (Han et al., 2014; Deng et al., 2018). This is supported by an analysis indicating that anthropogenic pollution was not the main contributor to the enhancement of OA, at least during the period 1200–1600 JST (Text S9), and by the report that primary biogenic OA is mainly in the supermicrometer aerosol diameter range in a forest environment, for the Amazon at least (Pöschl et al., 2010). Furthermore, the stronger enhancement of LOOA than of MOOA indicates that the freshly formed BSOA was mainly composed of LOOA and had a low oxygenation state. The O:C ratio of OA increased slowly from around noon to midnight (Fig. 2c), together with the appearance of MOOA, indicating the aging of freshly formed BSOA (Han et al., 2014). Because of high RH conditions (Fig. S7), aqueous phase reactions including in-cloud processes could have played an important role in the aging of fresh BSOA (Han et al., 2014), which could have modified the hygroscopicity of ambient aerosols (Jimenez et al., 2009; Farmer et al., 2015). Although no abrupt increase of sub-30 nm particles was observed, the increase in the number concentration of 30–50 nm particles around noon indicates the formation of new particles near the observation site. These particles probably had grown by the condensation of BSOA formed from BVOC at the time they were transported to the observation site. The concentrations of nitrate and chloride stayed low, although they also presented maxima in the afternoon. Sulfate, which may have been strongly influenced by transported anthropogenic aerosol, did not present an obvious diurnal variation. This result supports the view that the contribution of anthropogenic OA to the observed enhancement of OA was small.

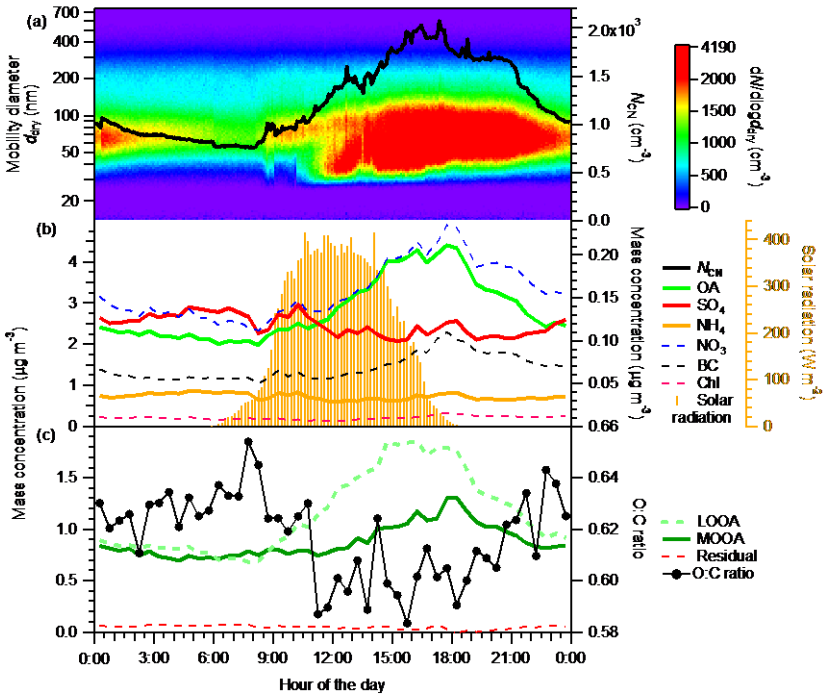

Figure 2: Diurnal variations of (a) number-size distribution (image plot) and number concentration (N_{CN}, right axis) of ambient aerosols, and the mass concentrations of (b) OA, SO_4, and NH_4 (left axis), and NO_3, BC, and Chl (right axis in black), and (c) LOOA, MOOA, and residual, and the O:C ratio of bulk OA (only data with m_{org} > 0.3 μg m^{-3} are included) averaged for the entire study period. (A box and whiskers plot of the diurnal variation of O:C ratio is presented in Fig. S19.) The diurnal variation of solar radiation averaged for the entire period is superimposed in panel (b).

4.1.2 Hygroscopicity of atmospheric aerosols

Similar to a prior observation at the same site in 2010 (Kawana et al., 2017), the hygroscopic growth factor g_f presented unimodal distributions at respective particle diameters (Figs. 1d, 1e, and S11), and the mean hygroscopic growth factor $g_{f,m}$ of the aerosols increased with increase of the particle diameters (Fig. S12). The mean ± SD of $g_{f,m}$ at 30, 50, 70, 100, 200, 300,

and 360 nm were 1.13 ± 0.08, 1.21 ± 0.09, 1.22 ± 0.09, 1.26 ± 0.10, 1.36 ± 0.10, 1.40 ± 0.08, and 1.42 ± 0.08, respectively. The unimodal pattern of the g_f-PDF indicated the internal mixing state of the observed aerosol at the respective particle diameters. Decreases of $g_{f,m}$ (Fig. S12) were observed for all particles during periods of intensive BSOA formation (i.e., episodes when the mass concentration of OA especially LOOA greatly increased; such episodes were observed on 31 August, and on 2, 5, 7, 9, 14, 15, 17, 18, 19, 20, and 21 September; Fig. 1b).

The hygroscopicity parameter of ambient aerosol particles that corresponds to $g_{f,mw}$ (κ_i) also increased with the increase of aerosol particle diameters (Fig. 3a). Similar diurnal variation patterns were observed for all the diameters studied. The κ_i started to decrease around 0800 JST, then reached daily minima between 1300 and 1900 JST. Then it increased continually until around 0200 JST of the next day, and remained high until 0800 JST the next morning. For particles with $d_{dry} \geq 100$ nm, the diurnal variation pattern and size-dependence of κ_i were opposite to those of the volume fraction of OA (Fig. 3b) and were similar to those of the volume fraction of total inorganic salts (Fig. S13). The results suggest that, at least for ambient aerosol particles with $d_{dry} \geq 100$ nm, OA and inorganic salts had low and high hygroscopicity, respectively, resulted in the variations of κ_i. Although $\kappa_{inorgsalt}$ is much greater than κ_{org} (Petters and Kreidenweis, 2007), the high ε_{org} makes the influence of OA on κ_i significant. Thus, the variation of κ_{org} (Sect. 4.2) may also contribute to the variation of κ_i. For particles with $d_{dry} \leq 70$ nm, decrease of the particle hygroscopicity with decrease of the particle diameter is also explained by the accompanying increase of ε_{org} and the decrease of $\varepsilon_{inorgsalt}$ (Levin et al., 2014). This is indicated by the substantially lower mean mass fraction of inorganic salts than of organics in the corresponding d_{va} range of less than 150 nm (Fig. S2). In particular, for particles with d_{dry} of 30 nm, κ_i remained constant in a low range (0.079–0.089) from 1300 JST to 1700 JST with a mean value of 0.082. BSOA formed during this period probably dominated the particle mass (Kawana et al., 2017; Han et al., 2014).

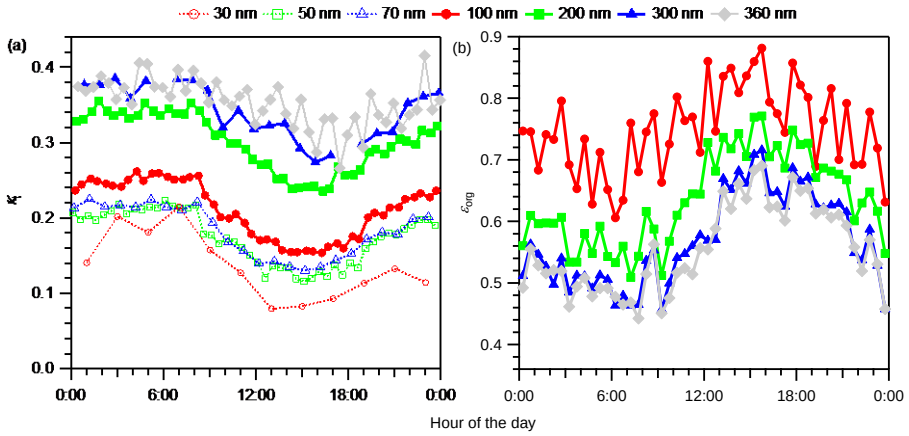

Figure 3: Diurnal variations of (a) size-resolved hygroscopicity of aerosols (κ) and (b) size-resolved volume fractions of OA (ε_{org}) for the entire study period. Note that for particles with d_{dry} of 30 nm, κ is presented in 2-h time resolution because of the low data coverage (Fig. S12).

4.2 Hygroscopicity of organic aerosol components

4.2.1 Variation of κ_{org} and its relation to the chemical structure of OA

The diurnal variation of κ_{org} and the volume fraction of LOOA in OA, $v_{LOOA}/(v_{LOOA}+v_{MOOA})$, where v_{LOOA} and v_{MOOA} refer to the volume concentrations of LOOA and MOOA, respectively, for the entire study period are presented in Fig. 4. Data with $\varepsilon_{org} < 0.40$ were excluded from the κ_{org} values presented because the uncertainty that originated from subtraction of the contribution of inorganic components was considered large in the low ε_{org} range (Mei et al., 2013a). The κ_{org} decreased rapidly from approximately 0800 JST in the morning when the mass concentrations of OA and LOOA started to increase (Fig. 2). The κ_{org} reached daily minima during 1000–1800 JST, and increased after the minima (Fig. 4a). The $v_{LOOA}/(v_{LOOA}+v_{MOOA})$ in Fig. 4b presents the opposite diurnal variation pattern. The characteristics of the size-dependence of κ_{org} and $v_{LOOA}/(v_{LOOA}+v_{MOOA})$ were dependent on time periods. To characterize the size-dependence of κ_{org} and $v_{LOOA}/(v_{LOOA}+v_{MOOA})$, the mean values of κ_{org} and $v_{LOOA}/(v_{LOOA}+v_{MOOA})$ during 1200–2000 JST and 2000–1200 JST were plotted separately in the κ_{org} - $v_{LOOA}/(v_{LOOA}+v_{MOOA})$

space for different d_{dry} (Fig. 5), and the difference in the diurnal variation data between particles with different diameters were evaluated using a 10 % two-sided t-test (Table S7). During 1200–2000 JST, opposite size-dependences were observed between the mean κ_{org} and $v_{LOOA}/(v_{LOOA}+v_{MOOA})$. Although the differences of κ_{org} between 200 and 300 nm particles (p-value: 0.71) and 300 and 360 nm particles (p-value: 0.15) were not significant, the differences of κ_{org} between 100 and 200 nm particles (p-value: 0.01) and 200 and 360 nm particles (p-value: 0.07), and the differences of $v_{LOOA}/(v_{LOOA}+v_{MOOA})$ between particles with all different diameters (p-value: <0.02), were significant during that period. During 2000–1200 JST, the size-dependences of κ_{org} and $v_{LOOA}/(v_{LOOA}+v_{MOOA})$ were not clear. The clearer size-dependence of both κ_{org} and $v_{LOOA}/(v_{LOOA}+v_{MOOA})$ during 1200–2000 JST than during 2000–1200 JST, was explained by the formation of BSOA during the afternoon hours. The patterns of diurnal variation and of size-dependence between κ_{org} and $v_{LOOA}/(v_{LOOA}+v_{MOOA})$ during 1200–2000 JST indicate that the variation of κ_{org} could be explained at least in part by the relative contributions of LOOA and MOOA to OA. That is, the presence of LOOA with low oxygenation state (O:C ratio of 0.47) lowered the observed κ_{org}, while the presence of MOOA with high oxygenation state (O:C ratio of 0.95) increased the observed κ_{org}. A similar relationship was observed in a former study at the observation site: κ_{org} was positively correlated with the O:C ratio of the organics (Deng et al., 2018).

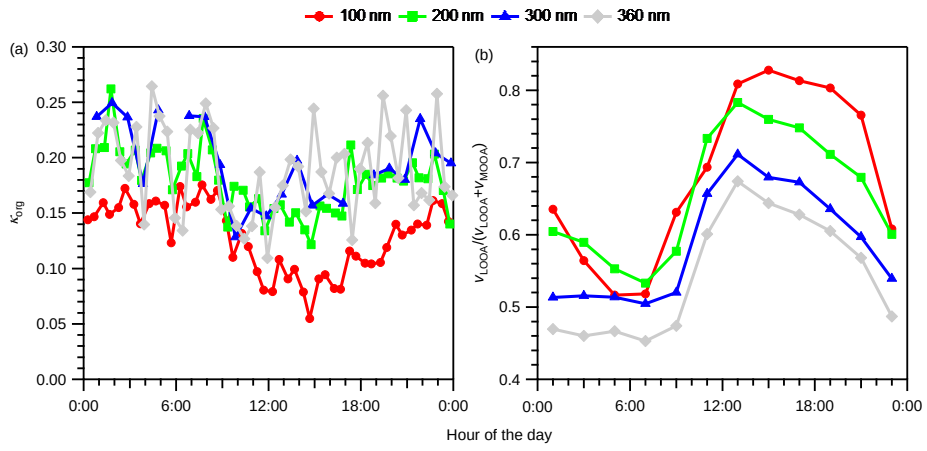

Figure 4: Diurnal variations of (a) size-resolved hygroscopicity of OA (κ_{org}) and (b) size-resolved volume fractions of LOOA in OA ($v_{LOOA}/(v_{LOOA}+v_{MOOA})$) for the entire study period. For κ_{org} in panel (a), only data with ε_{org} > 0.40 were considered. The values in panel (b) were calculated from the diurnal variations of the average volume concentrations of LOOA and MOOA (Fig. S16), not from the averages of $v_{LOOA}/(v_{LOOA}+v_{MOOA})$.

The hygroscopicity parameters of LOOA (κ_{LOOA}) and MOOA (κ_{MOOA}) were determined to evaluate the variations of κ_{org} that can be explained by the relative contributions of LOOA and MOOA to OA. For the determination of κ_{LOOA} and κ_{MOOA}, κ_{org} was plotted against $v_{LOOA}/(v_{LOOA}+v_{MOOA})$ and their correlation was analyzed based on linear regression analysis (Figs. 5 and S14). For particles with d_{dry} of 100, 200, 300, and 360 nm, the correlation coefficients between κ_{org} and $v_{LOOA}/(v_{LOOA}+v_{MOOA})$ were −0.50, −0.58, −0.27, and −0.099, respectively. Relatively high correlations were observed for particles with d_{dry} of 100 and 200 nm, probably because higher particle number concentrations (Fig. 1c) and higher OA volume fractions (Fig. 3) led to smaller uncertainties in the derived κ_{org} in those diameter ranges, than in those of 300 and 360 nm. The regression line for particles with d_{dry} of both 100 and 200 nm (Fig. 5) were used to derive κ_{LOOA} and κ_{MOOA} by applying $v_{LOOA}/(v_{LOOA}+v_{MOOA})$ of zero and unity to the obtained regression equation, respectively. The derived κ_{LOOA} and κ_{MOOA} were 0.083 and 0.28, respectively. This result is in between the results if particles with d_{dry} of only 100 nm (derived κ_{LOOA} and κ_{MOOA} were 0.060 and 0.25, respectively) and only 200 nm (derived κ_{LOOA} and κ_{MOOA} were 0.095 and 0.34, respectively) were used. Compared with the κ of PMF factors reported by Jimenez et al. (2009), the derived κ_{LOOA} and κ_{MOOA} are within the ranges of κ for semi-volatile oxygenated OA (0.04–0.18) and low-volatility oxygenated OA (0.18–0.35), respectively (Fig. 5). The size-resolved $v_{LOOA}/(v_{LOOA}+v_{MOOA})$ and the above derived κ_{LOOA} and κ_{MOOA} were used to reconstruct the diurnal variation data and mean values of size-resolved κ_{org} during 1200–2000 JST based on the volume additivity assumption. The reconstructed κ_{org} and the κ_{org} described above (measured κ_{org}) were compared and their correlations were evaluated through linear regression analysis (Fig. S15). The slope and r^2 of the regression line are used to assess the ability of LOOA and MOOA to explain the variations of κ_{org}. For 100 and 200 nm particles, the relative contribution of LOOA and MOOA to OA can explain the majority of the variations of κ_{org} (the slope and r^2 for 100 nm particles were 0.72 and 0.79, respectively and those for 200 nm particles were 0.63 and 0.68, respectively). The variations of κ_{org} of 300 and 360 nm particles are explained less by the relative contributions of LOOA and MOOA to OA (the slope and r^2 for 300 nm particles were 0.31 and 0.48, respectively; for 360 nm particles were 0.16 and 0.07, respectively). The slope and r^2 of the regression line between reconstructed and measured κ_{org} for particles with

all four d_{dry} were 0.39 and 0.44, respectively. This result indicates that the relative contribution of LOOA and MOOA can explain around 40 % of the observed diurnal variations of κ_{org}. The slope and r^2 of the regression line over the mean reconstructed and observed κ_{org} of the four different sizes during afternoon hours (1200–2000 JST) were 0.39 and 0.84, respectively, which indicates that the size-dependence of κ_{org} is explained by the relative contribution of LOOA and MOOA to OA by at least ~ 40 % during the time period.

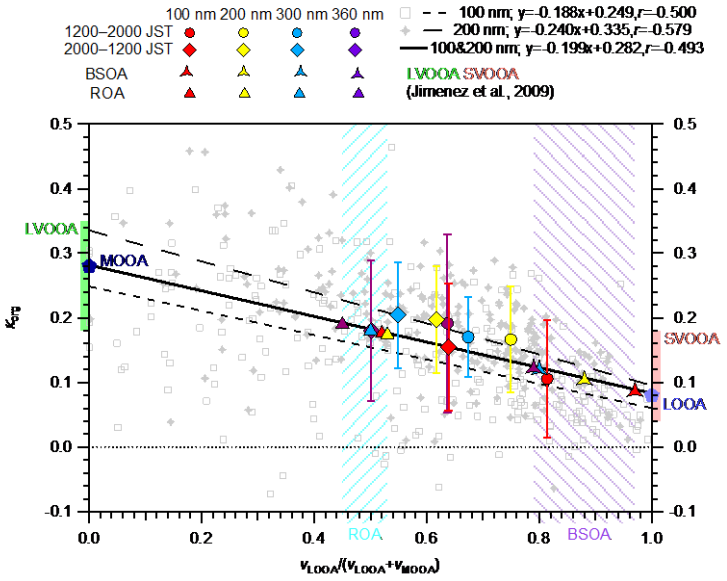

Figure 5: κ_{org} versus $v_{LOOA}/(v_{LOOA}+v_{MOOA})$ for particles with d_{dry} of 100 nm (gray open squares) and 200 nm (gray cross markers) over the entire study period. The time resolution of individual data is 2 h. Only data with ε_{org} > 0.40 are considered. The short-dashed, long-dashed, and solid lines are the regression lines for particles with d_{dry} of 100 nm, 200 nm, and the sum of the particles with the two sizes, respectively. The κ values of LOOA and MOOA derived from the regression lines (Sect. 4.2.1) are indicated by the light and dark blue pentagons, respectively. The size-resolved mean κ_{org} during 1200–2000 JST and 2000–1200 JST are indicated as filled circles and diamond markers, respectively. The standard deviations of the mean κ_{org} are indicated by the whiskers. The standard deviations of the mean $v_{LOOA}/(v_{LOOA}+v_{MOOA})$ are presented in Table S6. The size-resolved κ values of BSOA and ROA are indicated by the three-pointed stars and triangles, respectively. The diameters of κ_{org}, κ_{BSOA}, and κ_{ROA} are differentiated by colors. The ranges of κ for low-volatility oxygenated OA (LVOOA) and semi-volatile oxygenated OA (SVOOA) from Jimenez et al. (2009) are superimposed on the left and right axes, respectively. The shaded areas represent the estimated ranges of $v_{LOOA}/(v_{LOOA}+v_{MOOA})$ for ROA (left slash pattern) and BSOA (right slash pattern) of 100–360 nm particles.

4.2.2 Hygroscopicity of biogenic secondary organic aerosols

The hygroscopicity parameter of freshly formed BSOA (κ_{BSOA}) was calculated as the volume weighted mean of κ_{LOOA} and κ_{MOOA}. As discussed in Sect. 4.1.1, the enhanced OA mass in the daytime can be regarded as fresh BSOA. To simplify the analysis, the remaining part of the observed OA can be regarded as regionally transported OA (ROA), which may contain some aged, locally formed BSOA (Deng et al., 2018). To estimate the size-resolved contributions of LOOA and MOOA to BSOA and ROA, the size-resolved diurnal variations of sulfate was assumed as a tracer of regionally transported aerosol, and was scaled to represent the diurnal variations of LOOA and MOOA that constitute ROA (LOOA-ROA and MOOA-ROA; Fig. S16). For the scaling, the period of 0600–0800 JST, when OA and its subcomponents reached their daily minima (Figs. 2 and S16), was regarded as the background period, and all the LOOA and MOOA during the period were considered constituents of ROA. The remaining fractions of LOOA and MOOA were regarded as constituents of BSOA, referred to as LOOA-BSOA and MOOA-BSOA, respectively. The $v_{LOOA}/(v_{LOOA}+v_{MOOA})$ of ROA was estimated to be 0.52, 0.53, 0.50, and 0.45 for particles with d_{dry} of 100, 200, 300, and 360 nm, respectively (the range is presented by a left-slash pattern in Fig. 5). The period when the diurnal variations of the size-resolved concentration of LOOA reached their maxima (i.e., 1400–1600 JST; Fig. S16) was chosen to estimate the size-resolved $v_{LOOA}/(v_{LOOA}+v_{MOOA})$ of BSOA. The estimated $v_{LOOA}/(v_{LOOA}+v_{MOOA})$ of the BSOA were 0.97, 0.88, 0.80, and 0.79 for particles with d_{dry} of 100, 200, 300, and 360 nm, respectively (the range is presented by a right-slash pattern in Fig. 5). Although the estimated BSOA could have aged to some extent, it was defined as fresh BSOA. The κ_{BSOA} (and κ_{ROA}) were calculated using the derived $v_{LOOA}/(v_{LOOA}+v_{MOOA})$ of BSOA (ROA) for particles with different d_{dry} and κ_{LOOA} and κ_{MOOA}, and found to be 0.089 (0.18), 0.11 (0.18), 0.12 (0.18), and 0.12 (0.19) for particles with d_{dry} of 100, 200, 300, and 360 nm, respectively. The result indicates that κ_{BSOA} may increase with increase of the particle diameter as a result of the size-dependent contribution of LOOA and MOOA to BSOA (Fig. 5; colored three-pointed stars), which however needs to be confirmed by further studies. The size-dependence of the estimated κ_{ROA} (Fig. 5; colored triangles) was less obvious than that of κ_{BSOA}. The κ_{BSOA} derived at 85 % RH for particles with d_{dry} of 100 nm in this study (0.089) was slightly smaller than that in a previous study for particles with similar diameters under SUPS condition (0.10 at 94±11 nm) at the same site (Deng

et al., 2018). The derived κ_{ROA} is similar to the average κ_{org} during the nighttime (Fig. 4). The size-resolved volume concentrations of BSOA (v_{BSOA}) and ROA (v_{ROA}) were also estimated using those size-resolved $v_{LOOA}/(v_{LOOA}+v_{MOOA})$ values of BSOA and ROA (Text S10). The obtained volume fraction of BSOA in aerosol particles (ε_{BSOA}; Fig. S18) presented diurnal variation patterns that were similar to those of $v_{LOOA}/(v_{LOOA}+v_{MOOA})$. Furthermore, the size dependence of ε_{BSOA} during afternoon hours was also similar to that of $v_{LOOA}/(v_{LOOA}+v_{MOOA})$. Because both the volume concentrations and hygroscopicity of BSOA and ROA were derived from that of LOOA and MOOA, the variation of the relative contributions of the estimated BSOA and ROA to OA can explain 40 % of the diurnal variation and size-dependence of the measured κ_{org}.

4.3 Ranges of the variations of κ_t, κ_{org}, and κ_{BSOA}

The ranges of the diurnal variations of κ_t and κ_{org}, the difference between their maxima and minima, were obtained from their diurnal variation data with 2 h resolution (Table S8). The variation ranges of κ_t were 0.14, 0.091, 0.084, 0.10, 0.11, 0.11, and 0.070 for particles with d_{dry} of 30, 50, 70, 100, 200, 300, and 360 nm, respectively. The variation ranges of κ_{org} for particles with d_{dry} of 100, 200, 300, and 360 nm were 0.091, 0.079, 0.096, and 0.11, respectively. The size-dependence of κ_t and κ_{org} were quantified by the mean κ_t and κ_{org} values for the entire study period (Table S8). The difference of κ_t between particles with d_{dry} of 100 and 300 nm was 0.13, and that of κ_{org} was 0.056.

The ranges of both the diurnal variations and the size-dependence of κ_t are similar to those reported from a previous study at the same site in 2010 (the mean of the differences between 0900–2100 JST and 2100–0900 JST on NPF event days and on nonevent days for the d_{dry} range of 28.9–359 nm was in the range of 0.09–0.13, and the difference between Aitken mode and accumulation mode particles was 0.12) (Kawana et al., 2017), which pointed out the importance of the variation of particle hygroscopicity with time and size to the CCN number concentration. The ranges of both the diurnal variations and the size-dependence of κ_{org} are comparable to the range of 0.05 (from 0.08 to 0.13) that could lead to 30 % or more bias in the predicted CCN number concentration if not considered (Mei et al., 2013b). Here, only the ranges of the variation of κ_t and κ_{org} are discussed; other factors such as the absolute values of κ_t or κ_{org} should also be important to the prediction of CCN number concentrations. If SS is 0.1–1 %, typical maximum values in cloud systems (Farmer et al., 2015), the d_{dry} of 100 nm is close

to the mode diameters of the CCN number-size distributions in previous studies at the same site (Kawana et al., 2017; Deng et al., 2018). Whereas the d_{dry} of 300 nm is close to the mode mobility diameters of the mass-size distributions of OA and other aerosol components in this study (Fig. S2). The difference in the two types of mode diameters indicates that significant bias could be introduced if the bulk aerosol composition and/or OA composition is used for the prediction of CCN number concentrations.

The difference of the estimated κ_{BSOA} between particles with d_{dry} of 100 nm and 300 nm was estimated to be 0.031. The difference implies the importance of the size-dependence of κ_{BSOA} in the prediction of the contribution of BSOA to the CCN number concentration.

4.4 Contributions of OA and BSOA to CCN concentrations

The contributions of OA and BSOA to CCN number concentrations were assessed from the viewpoint of their contributions to the aerosol water uptake, which are size-dependent. For the estimate, the observed aerosols were assumed to be internally mixed. This is supported by a result from a previous study at the observation site: there was almost no difference in the prediction of the number fractions of CCN between the use of time- and size-resolved g_f distributions and time- and size-resolved $g_{f,m}$ (Kawana et al., 2017). The CCN activation diameters (d_{act}) for respective 2 h time bins of day at 0.4 % SS were calculated from reconstructed hygroscopicity parameter values of aerosol particles based on κ-Köhler theory (Text S11). The estimated total CCN number concentration is referred to as $N_{CCN,t}$. For each size range, the contribution of OA (BSOA) to the aerosol water uptake was represented as the product of the volume fraction of OA (BSOA) and κ_{org} (κ_{BSOA}) divided by κ_i [i.e., $\varepsilon_{org}\kappa_{org}/\kappa_i$ ($\varepsilon_{BSOA}\kappa_{BSOA}/\kappa_i$)], and was used to represent the fractional contribution of OA (and BSOA) to $dN_{CN}/d\log d_{dry}$ in the size range. The fractional contribution of OA (and BSOA) to $N_{CCN,t}$, hereafter referred to as $F_{CCN,OA}$ ($F_{CCN,BSOA}$), was derived by integrating the product of $dN_{CN}/d\log d_{dry}$ and $\varepsilon_{org}\kappa_{org}/\kappa_i$ ($\varepsilon_{BSOA}\kappa_{BSOA}/\kappa_i$) above the d_{act} and by dividing the obtained value by $N_{CCN,t}$. Details for the estimation of $F_{CCN,OA}$ and $F_{CCN,BSOA}$ are presented in Text S11.

Deleted: In two previous observations at the same site, the average CCN activation diameters of aerosols under 0.41 and 0.42 % SS were 71 and 68 nm, respectively (Kawana et al., 2017; Deng et al., 2018). Based on these facts, all the particles with d_{dry} greater than 70 nm were assumed to be CCN active.

Deleted: (Text S11)

Deleted: CCN activation diameter (70 nm)

Deleted: The diurnal variation of the CCN activation diameter was not considered for the estimate of $F_{CCN,OA}$ and $F_{CCN,BSOA}$ (Text S12).

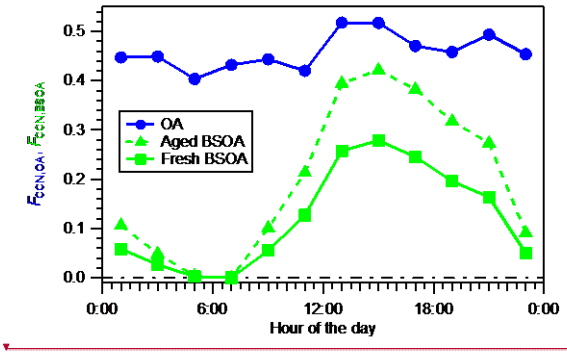

Figure 6: Diurnal variation of the fractional contribution of OA to the total CCN number concentration ($F_{CCN,OA}$) estimated using time- and size-resolved κ_{org}, and diurnal variation of the fractional contribution of BSOA to the total CCN number concentration ($F_{CCN,BSOA}$) estimated assuming fresh BSOA (using size-resolved κ_{BSOA}) and aged BSOA (using size-resolved κ_{ROA}).

The diurnal variation of $F_{CCN,OA}$ estimated using time- and size-resolved κ_{org} and that of $F_{CCN,BSOA}$ using size-resolved k_{BSOA} are presented in Fig. 6. Both $F_{CCN,OA}$ and $F_{CCN,BSOA}$ reached their maxima during 1200–1600 JST, when intensive BSOA formation was observed. The magnitude of the variation of $F_{CCN,BSOA}$ (from 0.00 to 0.28) was larger than that of $F_{CCN,OA}$ (from 0.40 to 0.52). This is explained by the larger magnitude of the diurnal variation range of ε_{BSOA} (Fig. S18), compared to that of ε_{org} (Fig. 3). The $F_{CCN,BSOA}$ of 0.28 during 1400–1600 JST indicates a significant contribution of BSOA to the CCN number concentration.

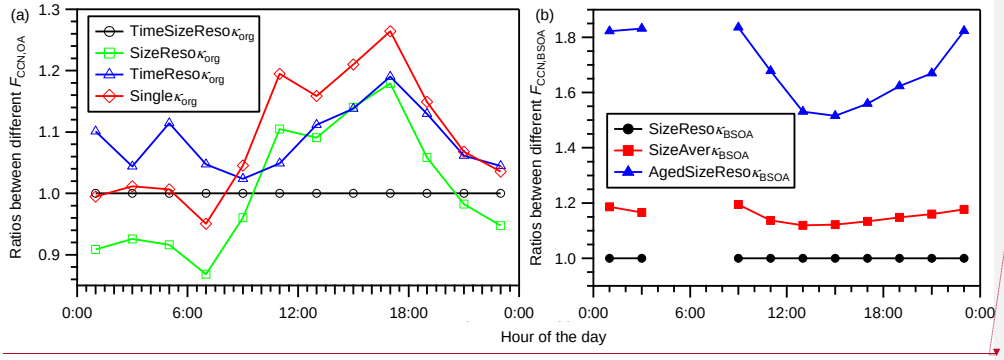

Deleted:

Deleted: 53

Deleted: 1200

Deleted:

Figure 7: (a) Diurnal variation of the ratios of the $F_{CCN,OA}$ derived using time- and size-resolved κ_{org} (TimeSizeResoκ_{org}), time-averaged and size-resolved κ_{org} (SizeResoκ_{org}), size-averaged and time-resolved κ_{org} (TimeResoκ_{org}), and time- and size-averaged κ_{org} (Singleκ_{org}) to that derived using the time- and size- resolved κ_{org} (TimeSizeResoκ_{org}). (b) Diurnal variation of the ratios of the $F_{CCN,BSOA}$ derived using size-resolved κ_{BSOA} (SizeResoκ_{BSOA}), size-averaged κ_{BSOA} (SizeAverκ_{BSOA}), and aged size-resolved κ_{BSOA} (AgedSizeResoκ_{BSOA}) to that derived using the size-resolved κ_{BSOA} (SizeResoκ_{BSOA}). In panel (b), the condition of aged size-resolved κ_{BSOA} assumes that the value of κ_{BSOA} equals that of κ_{ROA}, and the data during 0400–0800 JST, when the concentration of BSOA was low (volume concentration less than 0.01×10^{-6} cm^3 m^{-3}), are not presented (data are presented in Table S12).

Deleted: ; Fig. S18

Because obvious diurnal variations and size-dependence of κ_{org} were found and because κ_{BSOA} was also estimated to be size-dependent (Sect. 4.2), the sensitivities of the estimated $F_{CCN,OA}$ and $F_{CCN,BSOA}$ on the variations of κ_{org} and κ_{BSOA} were assessed. To assess the influence of the variation of κ_{org} on $F_{CCN,OA}$, the diurnal variations of $F_{CCN,OA}$ was estimated using (0a, base case) time- and size-resolved κ_{org}, (1a) size-resolved, time-averaged (note that the average here refers to the arithmetic mean, it is the same in other places of this paragraph) κ_{org}, (2a) time-resolved, size-averaged κ_{org}, and (3a) time- and size-averaged κ_{org} (Table S10). Cases (1a)–(3a) were compared with the base case (0a), as presented in Fig. 7a. Using time-averaged κ_{org} (case 1a), the $F_{CCN,OA}$ was overestimated by 18 % during 1600–1800 JST and underestimated by 13 % during 0600–0800 JST. Using size-averaged κ_{org} (case 2a), the $F_{CCN,OA}$ was overestimated by 2–19 % on a diurnal basis. Using time- and size-averaged κ_{org} (i.e., a single mean κ_{org}, case 3a), $F_{CCN,OA}$ was overestimated by 26 % during 1600–1800 JST and underestimated by 5.0 % during 0600–0800 JST. The deviation of case (3a) from the base case (0a) resulted from the factors leading to the deviations of cases (1a) and (2a). The magnitudes of the deviations, defined here as the difference between the lowest and highest values of the ratios in Fig. 7a, for (1a), (2a), and (3a) are 31, 17, and 31 %, respectively. The substantial differences suggest that the diurnal variations and size-dependence of κ_{org} are important for accurate prediction of the contribution of OA to the CCN number concentration in modelling studies. To assess the influence of the size-dependence of κ_{BSOA} on $F_{CCN,BSOA}$, the diurnal variations of $F_{CCN,BSOA}$ was estimated using (0b, base case) size-resolved κ_{BSOA} and (1b) size-averaged κ_{BSOA} (Table S11). Case (1b) was compared with case (0b), as presented in Fig. 7b. Using size-averaged κ_{BSOA} caused overestimation of $F_{CCN,BSOA}$ by 12–19 %, which relates to the decrease of the estimated κ_{BSOA} and the increase of $dN_{CN}/d\log d_{dry}$ (Fig. S17) with decrease in the dry particle diameter.

Deleted: 12

Deleted: 4.9

Deleted: 30

Furthermore, because fresh BSOA probably become aged after atmospheric transport, the influence of the aging of the estimated fresh BSOA (assuming κ_{BSOA} for the calculation of d_{act} and $F_{CCN,BSOA}$ was as large as that of κ_{ROA} (Table S11)) on

$F_{CCN,BSOA}$ was also evaluated. Here, the estimation of $F_{CCN,BSOA}$ in the aged condition ignored the possible change in the aerosol size distribution accompanying the aging process. Aged BSOA can contribute more to the aerosol water uptake and thus to the CCN number concentration. Assuming that the BSOA was as aged as ROA, the estimated $F_{CCN,BSOA}$ was 52–84 % larger than that estimated assuming fresh BSOA (Fig. 7b), and it could have been 0.42 if the aerosol observed during 1400–1600 JST aged (Fig. 6). The result suggests that, whereas the contribution of BSOA to CCN was substantial at the study site, the magnitude of the contribution might be increased substantially by aging of the BSOA during transport after its formation in the forest.

Deleted: CCN activation diameter accompanying the aging processes (Text S13). The possible change in the

Deleted: was also not considered here

Deleted: 50

Deleted: 43

5 Summary and conclusions

The size-resolved hygroscopicity at 85 % RH, chemical composition, and number-size distributions of atmospheric aerosols were observed at a forest site in Wakayama, Japan in August and September, 2015. The diurnal variation and size-dependence in the hygroscopicity of the observed aerosol and organic aerosol components (OA) were discussed in view of the formation of BSOA. The fractional contributions of OA and BSOA to the total CCN number concentration were discussed in view of the variations of the hygroscopicity parameter of OA and BSOA.

Similar to two previous observations at the same site (Han et al., 2013, 2014; Kawana et al., 2017; Deng et al., 2018), OA was the dominant sub-micrometer aerosol component, followed by sulfate. While the mass concentration of sulfate, on average, did not vary much in a day, the mass concentration of OA increased substantially in the afternoon hours, which was presumably explained by the condensation of BSOA. The hygroscopicity of ambient aerosol (κ_i) and of OA (κ_{org}) increased with increase of the dry particle diameter and presented daily minima in the afternoon hours. In this study, the ranges of the diurnal variations of κ_{org} of 100–360 nm particles were 0.079–0.11 and the κ_{org} of 300 nm particles was 0.056 larger than that of the 100 nm particles. The diurnal variations and size-dependence of κ_i can be explained by the relative contributions of OA and inorganic salts in the observed aerosol. The relative contributions of the estimated fresh BSOA and regional OA can explain 40 % of the diurnal variation and size-dependence of κ_{org}. The hygroscopicity of fresh BSOA (κ_{BSOA}) was estimated to increase (0.089–0.12) with increase of the dry particle diameter (100–300 nm).

The fractional contributions of OA and fresh BSOA to CCN number concentrations estimated from the viewpoint of their contributions to the water uptake by the aerosol were in the ranges 0.40–0.52 and 0.00–0.28, respectively. Compared with the

Deleted: 53

use of time- and size-resolved κ_{org}, the use of time- and size-averaged κ_{org} overestimated the contribution of OA to the CCN number concentration by up to 26 % (1600–1800 JST) and underestimated the contribution by up to 5.0 % (0600–0800 JST). These results indicate the importance of the diurnal variations and size-dependence of κ_{org} in the prediction of the contribution of OA to the CCN number concentration. The use of size-averaged κ_{BSOA} overestimated the contribution of fresh BSOA to the CCN number concentration by 12–19 % compared with the use of size-resolved κ_{BSOA}. If aging of BSOA after atmospheric transport occurs, the contribution of fresh BSOA to the CCN number concentration could be increased by 52–84 %, and could have reached a high value of 0.42 if the aerosol observed during 1400–1600 JST aged.

Deleted: 4.9

Deleted: 50

Deleted: 43

This study revealed the large magnitude of the diurnal variation and size-dependence of κ_{org} at the observation site under the influence of the formation of BSOA. Also revealed was the importance of the variation of κ_{org} to the estimation of the contribution of OA to the CCN number concentration from the viewpoint of the size-resolved contribution of OA to the water uptake of aerosols. Because both the diurnal variation and size-dependence of κ_{org} in the studied forest are different from those in some other forest environments (Cerully et al., 2015; Thalman et al., 2017), further studies on the variation of the hygroscopicity of organics and on the contributions of OA and BSOA to the CCN concentrations should be performed in other forest environments. Furthermore, the size-dependence of the hygroscopicity of fresh BSOA estimated here should be confirmed by additional studies.

Data availability. All of the final derived data supporting the findings of this study are available in the article or in its supporting information file.

Author contributions. MM and YD designed the experiments, and YD, HY, MM, HF, and TN performed them. YD analyzed the data with contributions from MM, TN, and KK. YD prepared the manuscript with contributions from MM, KK, and TN.

Competing interests. The authors declare that they have no conflict of interest.

Acknowledgements. We thank the faculty and staff of the Wakayama Forest Research Station, Field Science Education and Research Center of Kyoto University, Japan, for the provision of the study site and the meteorological data. We thank Qingcai Chen, Kouji Adachi, Yuuki Kuruma, Ryuji Fujimori, and Takayuki Yamasaki for their help in the field observation. We acknowledge Kazuma Aoki for the use of the 1λ-PSAP instrument. We acknowledge the NOAA Air Resources Laboratory

(ARL) for providing the HYSPLIT transport and dispersion model. This study was supported in part by JSPS KAKENHI Grant Numbers JP26281007 and JP18K19852.

References

Bougiatioti, A., Bezantakos, S., Stavroulas, I., Kalivitis, N., Kokkalis, P., Biskos, G., Mihalopoulos, N., Papayannis, A., and Nenes, A.: Biomass-burning impact on CCN number, hygroscopicity and cloud formation during summertime in the eastern Mediterranean, Atmospheric Chemistry and Physics, 16, 7389-7409, 10.5194/acp-16-7389-2016, 2016.

Cerully, K. M., Bougiatioti, A., Hite, J. R., Guo, H., Xu, L., Ng, N. L., Weber, R., and Nenes, A.: On the link between hygroscopicity, volatility, and oxidation state of ambient and water-soluble aerosols in the southeastern United States, Atmospheric Chemistry and Physics, 15, 8679-8694, 10.5194/acp-15-8679-2015, 2015.

Clegg, S. L., Brimblecombe, P., and Wexler, A. S.: Thermodynamic model of the system H+-NH4+-SO42−-NO3−-H2O at tropospheric temperatures, Journal of Physical Chemistry A, 102, 2137-2154, 10.1021/jp973042r, 1998.

Deng, Y. G., Kagami, S., Ogawa, S., Kawana, K., Nakayama, T., Kubodera, R., Adachi, K., Hussein, T., Miyazaki, Y., and Mochida, M.: Hygroscopicity of Organic Aerosols and Their Contributions to CCN Concentrations Over a Midlatitude Forest in Japan, Journal of Geophysical Research-Atmospheres, 123, 9703-9723, 10.1029/2017jd027292, 2018.

Draxier, R. R., and Hess, G. D.: An overview of the HYSPLIT_4 modelling system for trajectories, dispersion and deposition, Australian Meteorological Magazine, 47, 295-308, 1998.

Ehn, M., Thornton, J. A., Kleist, E., Sipila, M., Junninen, H., Pullinen, I., Springer, M., Rubach, F., Tillmann, R., Lee, B., Lopez-Hilfiker, F., Andres, S., Acir, I. H., Rissanen, M., Jokinen, T., Schobesberger, S., Kangasluoma, J., Kontkanen, J., Nieminen, T., Kurten, T., Nielsen, L. B., Jorgensen, S., Kjaergaard, H. G., Canagaratna, M., Dal Maso, M., Berndt, T., Petaja, T., Wahner, A., Kerminen, V. M., Kulmala, M., Worsnop, D. R., Wildt, J., and Mentel, T. F.: A large source of low-volatility secondary organic aerosol, Nature, 506, 476-+, 10.1038/nature13032, 2014.

Farmer, D. K., Cappa, C. D., and Kreidenweis, S. M.: Atmospheric processes and their controlling influence on cloud condensation nuclei activity, Chemical Reviews, 115, 4199-4217, 10.1021/cr5006292, 2015.

Frosch, M., Bilde, M., DeCarlo, P. F., Juranyi, Z., Tritscher, T., Dommen, J., Donahue, N. M., Gysel, M., Weingartner, E., and Baltensperger, U.: Relating cloud condensation nuclei activity and oxidation level of alpha-pinene secondary organic aerosols, Journal of Geophysical Research-Atmospheres, 116, 9, 10.1029/2011jd016401, 2011.

Frosch, M., Bilde, M., Nenes, A., Praplan, A. P., Juranyi, Z., Dommen, J., Gysel, M., Weingartner, E., and Baltensperger, U.: CCN activity and volatility of beta-caryophyllene secondary organic aerosol, Atmospheric Chemistry and Physics, 13, 2283-2297, 10.5194/acp-13-2283-2013, 2013.

Han, Y. M., Iwamoto, Y., Nakayama, T., Kawamura, K., Hussein, T., and Mochida, M.: Observation of new particle formation over a mid-latitude forest facing the North Pacific, Atmospheric Environment, 64, 77-84, 10.1016/j.atmosenv.2012.09.036, 2013.

Han, Y. M., Iwamoto, Y., Nakayama, T., Kawamura, K., and Mochida, M.: Formation and evolution of biogenic secondary organic aerosol over a forest site in Japan, Journal of Geophysical Research-Atmospheres, 119, 259-273, 10.1002/2013jd020390, 2014.

Jimenez, J. L., Canagaratna, M. R., Donahue, N. M., Prevot, A. S. H., Zhang, Q., Kroll, J. H., DeCarlo, P. F., Allan, J. D., Coe, H., Ng, N. L., Aiken, A. C., Docherty, K. S., Ulbrich, I. M., Grieshop, A. P., Robinson, A. L., Duplissy, J., Smith, J. D., Wilson, K. R., Lanz, V. A., Hueglin, C., Sun, Y. L., Tian, J., Laaksonen, A., Raatikainen, T., Rautiainen, J., Vaattovaara, P., Ehn, M., Kulmala, M., Tomlinson, J. M., Collins, D. R., Cubison, M. J., Dunlea, E. J., Huffman, J. A., Onasch, T. B., Alfarra, M. R.,

Williams, P. I., Bower, K., Kondo, Y., Schneider, J., Drewnick, F., Borrmann, S., Weimer, S., Demerjian, K., Salcedo, D., Cottrell, L., Griffin, R., Takami, A., Miyoshi, T., Hatakeyama, S., Shimono, A., Sun, J. Y., Zhang, Y. M., Dzepina, K., Kimmel, J. R., Sueper, D., Jayne, J. T., Herndon, S. C., Trimborn, A. M., Williams, L. R., Wood, E. C., Middlebrook, A. M., Kolb, C. E., Baltensperger, U., and Worsnop, D. R.: Evolution of Organic Aerosols in the Atmosphere, Science, 326, 1525-1529, 10.1126/science.1180353, 2009.

Kawana, K., Nakayama, T., and Mochida, M.: Hygroscopicity and CCN activity of atmospheric aerosol particles and their relation to organics: Characteristics of urban aerosols in Nagoya, Japan, Journal of Geophysical Research-Atmospheres, 121, 4100-4121, 10.1002/2015jd023213, 2016.

Kawana, K., Nakayama, T., Kuba, N., and Mochida, M.: Hygroscopicity and cloud condensation nucleus activity of forest aerosol particles during summer in Wakayama, Japan, Journal of Geophysical Research-Atmospheres, 122, 3042-3064, 10.1002/2016jd025660, 2017.

Kondo, Y., Sahu, L., Kuwata, M., Miyazaki, Y., Takegawa, N., Moteki, N., Imaru, J., Han, S., Nakayama, T., Oanh, N. T. K., Hu, M., Kim, Y. J., and Kita, K.: Stabilization of the Mass Absorption Cross Section of Black Carbon for Filter-Based Absorption Photometry by the use of a Heated Inlet, Aerosol Science and Technology, 43, 741-756, 10.1080/02786820902889879, 2009.

Kyoto University: Kenkyurin · Shikenchi Joho 2010, in: Sections of Forest Station Management and Field Station Management, Field Science Education and Research Center, Kyoto University, Japan (in Japanese), 2017.

Levin, E. J. T., Prenni, A. J., Palm, B. B., Day, D. A., Campuzano-Jost, P., Winkler, P. M., Kreidenweis, S. M., DeMott, P. J., Jimenez, J. L., and Smith, J. N.: Size-resolved aerosol composition and its link to hygroscopicity at a forested site in Colorado, Atmospheric Chemistry and Physics, 14, 2657-2667, 10.5194/acp-14-2657-2014, 2014.

Liu, X. H., and Wang, J. A.: How important is organic aerosol hygroscopicity to aerosol indirect forcing?, Environmental Research Letters, 5, 10, 10.1088/1748-9326/5/4/044010, 2010.

McFiggans, G., Artaxo, P., Baltensperger, U., Coe, H., Facchini, M. C., Feingold, G., Fuzzi, S., Gysel, M., Laaksonen, A., Lohmann, U., Mentel, T. F., Murphy, D. M., O'Dowd, C. D., Snider, J. R., and Weingartner, E.: The effect of physical and chemical aerosol properties on warm cloud droplet activation, Atmospheric Chemistry and Physics, 6, 2593-2649, 10.5194/acp-6-2593-2006, 2006.

McNeill, V. F.: Aqueous Organic Chemistry in the Atmosphere: Sources and Chemical Processing of Organic Aerosols, Environmental Science & Technology, 49, 1237-1244, 10.1021/es5043707, 2015.

Mei, F., Hayes, P. L., Ortega, A., Taylor, J. W., Allan, J. D., Gilman, J., Kuster, W., de Gouw, J., Jimenez, J. L., and Wang, J.: Droplet activation properties of organic aerosols observed at an urban site during CalNex-LA, Journal of Geophysical Research-Atmospheres, 118, 2903-2917, 10.1002/jgrd.50285, 2013a.

Mei, F., Setyan, A., Zhang, Q., and Wang, J.: CCN activity of organic aerosols observed downwind of urban emissions during CARES, Atmospheric Chemistry and Physics, 13, 12155-12169, 10.5194/acp-13-12155-2013, 2013b.

Mochida, M., Nishita-Hara, C., Kitamori, Y., Aggarwal, S. G., Kawamura, K., Miura, K., and Takami, A.: Size-segregated measurements of cloud condensation nucleus activity and hygroscopic growth for aerosols at Cape Hedo, Japan, in spring 2008, Journal of Geophysical Research-Atmospheres, 115, 16, 10.1029/2009jd013216, 2010.

Okumura, M.: Estimation of volatile organic compound emissions from forest vegetation, Ph.D. thesis, Graduate School of Energy Science, Kyoto University, Kyoto, Japan, 2009.

Paatero, P., and Tapper, U.: Positive matrix factorization - a nonnegative factor model with optimal utilization of error-estimates of data values, Environmetrics, 5, 111-126, 10.1002/env.3170050203, 1994.

Petters, M. D., and Kreidenweis, S. M.: A single parameter representation of hygroscopic growth and cloud condensation nucleus activity, Atmospheric Chemistry and Physics, 7, 1961-1971, 10.5194/acp-7-1961-2007, 2007.

Poschl, U., Martin, S. T., Sinha, B., Chen, Q., Gunthe, S. S., Huffman, J. A., Borrmann, S., Farmer, D. K., Garland, R. M., Helas, G., Jimenez, J. L., King, S. M., Manzi, A., Mikhailov, E., Pauliquevis, T., Petters, M. D., Prenni, A. J., Roldin, P., Rose, D., Schneider, J., Su, H., Zorn, S. R., Artaxo, P., and Andreae, M. O.: Rainforest Aerosols as Biogenic Nuclei of Clouds and Precipitation in the Amazon, Science, 329, 1513-1516, 10.1126/science.1191056, 2010.

Rastak, N., Pajunoja, A., Navarro, J. C. A., Ma, J., Song, M., Partridge, D. G., Kirkevag, A., Leong, Y., Hu, W. W., Taylor, N. F., Lambe, A., Cerully, K., Bougiatioti, A., Liu, P., Krejci, R., Petaja, T., Percival, C., Davidovits, P., Worsnop, D. R., Ekman, A. M. L., Nenes, A., Martin, S., Jimenez, J. L., Collins, D. R., Topping, D. O., Bertram, A. K., Zuend, A., Virtanen, A., and Riipinen, I.: Microphysical explanation of the RH-dependent water affinity of biogenic organic aerosol and its importance for climate, Geophysical Research Letters, 44, 5167-5177, 10.1002/2017gl073056, 2017.

Shingler, T., Crosbie, E., Ortega, A., Shiraiwa, M., Zuend, A., Beyersdorf, A., Ziemba, L., Anderson, B., Thornhill, L., Perring, A. E., Schwarz, J. P., Campazano-Jost, P., Day, D. A., Jimenez, J. L., Hair, J. W., Mikoviny, T., Wisthaler, A., and Sorooshian, A.: Airborne characterization of subsaturated aerosol hygroscopicity and dry refractive index from the surface to 6.5km during the SEAC(4)RS campaign, Journal of Geophysical Research-Atmospheres, 121, 4188-4210, 10.1002/2015jd024498, 2016.

Thalman, R., de Sa, S. S., Palm, B. B., Barbosa, H. M. J., Pohlker, M. L., Alexander, M. L., Brito, J., Carbone, S., Castillo, P., Day, D. A., Kuang, C. G., Manzi, A., Ng, N. L., Sedlacek, A. J., Souza, R., Springston, S., Watson, T., Pohlker, C., Poschl, U., Andreae, M. O., Artaxo, P., Jimenez, J. L., Martin, S. T., and Wang, J.: CCN activity and organic hygroscopicity of aerosols downwind of an urban region in central Amazonia: seasonal and diel variations and impact of anthropogenic emissions, Atmospheric Chemistry and Physics, 17, 11779-11801, 10.5194/acp-17-11779-2017, 2017.

Titos, G., Cazorla, A., Zieger, P., Andrews, E., Lyamani, H., Granados-Munoz, M. J., Olmo, F. J., and Alados-Arboledas, L.: Effect of hygroscopic growth on the aerosol light-scattering coefficient: A review of measurements, techniques and error sources, Atmospheric Environment, 141, 494-507, 10.1016/j.atmosenv.2016.07.021, 2016.

Tritscher, T., Dommen, J., DeCarlo, P. F., Gysel, M., Barmet, P. B., Praplan, A. P., Weingartner, E., Prevot, A. S. H., Riipinen, I., Donahue, N. M., and Baltensperger, U.: Volatility and hygroscopicity of aging secondary organic aerosol in a smog chamber, Atmospheric Chemistry and Physics, 11, 11477-11496, 10.5194/acp-11-11477-2011, 2011.

Tunved, P., Hansson, H. C., Kerminen, V. M., Strom, J., Dal Maso, M., Lihavainen, H., Viisanen, Y., Aalto, P. P., Komppula, M., and Kulmala, M.: High natural aerosol loading over boreal forests, Science, 312, 261-263, 10.1126/science.1123052, 2006.

Ulbrich, I. M., Canagaratna, M. R., Zhang, Q., Worsnop, D. R., and Jimenez, J. L.: Interpretation of organic components from Positive Matrix Factorization of aerosol mass spectrometric data, Atmospheric Chemistry and Physics, 9, 2891-2918, 10.5194/acp-9-2891-2009, 2009.

Vaishya, A., Ovadnevaite, J., Bialek, J., Jennings, S. G., Ceburnis, D., and O'Dowd, C. D.: Bistable effect of organic enrichment on sea spray radiative properties, Geophysical Research Letters, 40, 6395-6398, 10.1002/2013gl058452, 2013.

Vargaftik, N. B., Volkov, B. N., and Voljak, L. D.: INTERNATIONAL TABLES OF THE SURFACE-TENSION OF WATER, Journal of Physical and Chemical Reference Data, 12, 817-820, 10.1063/1.555688, 1983.

Wang, J., Lee, Y. N., Daum, P. H., Jayne, J., and Alexander, M. L.: Effects of aerosol organics on cloud condensation nucleus (CCN) concentration and first indirect aerosol effect, Atmospheric Chemistry and Physics, 8, 6325-6339, 10.5194/acp-8-6325-2008, 2008.

Wexler, A. S., and Clegg, S. L.: Atmospheric aerosol models for systems including the ions H+, NH4+, Na+, SO42−, NO3−, Cl−, Br−, and H2O, Journal of Geophysical Research-Atmospheres, 107, 14, 10.1029/2001jd000451, 2002.

Winkler, P. M., Ortega, J., Karl, T., Cappellin, L., Friedli, H. R., Barsanti, K., McMurry, P. H., and Smith, J. N.: Identification of the biogenic compounds responsible for size-dependent nanoparticle growth, Geophysical Research Letters, 39, 6, 10.1029/2012gl053253, 2012.

Yu, H., Ortega, J., Smith, J. N., Guenther, A. B., Kanawade, V. P., You, Y., Liu, Y. Y., Hosman, K., Karl, T., Seco, R., Geron, C., Pallardy, S. G., Gu, L. H., Mikkila, J., and Lee, S. H.: New Particle Formation and Growth in an Isoprene-Dominated

Ozark Forest: From Sub-5 nm to CCN-Active Sizes, Aerosol Science and Technology, 48, 1285-1298, 10.1080/02786826.2014.984801, 2014.

Zhang, Q., Jimenez, J. L., Canagaratna, M. R., Ulbrich, I. M., Ng, N. L., Worsnop, D. R., and Sun, Y. L.: Understanding atmospheric organic aerosols via factor analysis of aerosol mass spectrometry: a review, Analytical and Bioanalytical Chemistry, 401, 3045-3067, 10.1007/s00216-011-5355-y, 2011.

Zhao, D. F., Buchholz, A., Kortner, B., Schlag, P., Rubach, F., Kiendler-Scharr, A., Tillmann, R., Wahner, A., Flores, J. M., Rudich, Y., Watne, A. K., Hallquist, M., Wildt, J., and Mentel, T. F.: Size-dependent hygroscopicity parameter (κ) and chemical composition of secondary organic cloud condensation nuclei, Geophysical Research Letters, 42, 10920-10928, 10.1002/2015gl066497, 2015.

Zhao, Y., Wingen, L. M., Perraud, V., and Finlayson-Pitts, B. J.: Phase, composition, and growth mechanism for secondary organic aerosol from the ozonolysis of alpha-cedrene, Atmospheric Chemistry and Physics, 16, 3245-3264, 10.5194/acp-16-3245-2016, 2016.

Zhou, L., Gierens, R., Sogachev, A., Mogensen, D., Ortega, J., Smith, J. N., Harley, P. C., Prenni, A. J., Levin, E. J. T., Turnipseed, A., Rusanen, A., Smolander, S., Guenther, A. B., Kulmala, M., Karl, T., and Boy, M.: Contribution from biogenic organic compounds to particle growth during the 2010 BEACHON-ROCS campaign in a Colorado temperate needleleaf forest, Atmospheric Chemistry and Physics, 15, 8643-8656, 10.5194/acp-15-8643-2015, 2015.

Text S1. Performance check of the DMAs

Before and after the atmospheric observation, the accuracy of the sizing by three DMAs was assessed using standard size PSL particles (JSR SIZE STANDARD PARTICLES: SC-0055-D, SC-0100-D, and SC-032-S; Thermo Scientific^{TM}: 3500A). The mode diameters from fittings for the measurement data (Kawana et al., 2014) were compared with the manufacturer warranty (Table S1), which is interpreted as prescribed ranges of mean diameter ± the expanded uncertainty (k = 2). The mode diameters after the atmospheric observation agreed with those before the observation within 0.84 %. The results obtained before the atmospheric observation are as follows. For DMA1, whereas the measured mode diameter of SC-0100-D was within the prescribed range, the measured mode diameters of SC-0055-D and SC-032-S were 1.0 % larger than the upper end of the prescribed range and 0.76 % lower than the lower end of the prescribed range, respectively. For DMA2, the measured mode diameter of SC-0055-D was 1.5 % larger than the upper end of the prescribed range, and the measured mode diameters of SC-0100-D, SC-032-S, and 3500A were 0.85, 3.2, and 2.2 % lower than the lower end of the prescribed ranges, respectively. For DMA3, the measured mode diameter of SC-0055-D was 6.9 % larger than the upper end of the prescribed diameter range, and the measured mode diameters for all three of the other PSL standards were within the prescribed ranges.

Text S2. Performance check of HTDMA using ammonium sulfate particles

Before the atmospheric observation, an aqueous solution of ammonium sulfate (AS) (99.999 % purity, Sigma-Aldrich) was nebulized and the generated aerosols were dried and introduced to the HTDMA to assess the difference in the sizing between the two DMAs under dry condition and to validate the control of RH in the HTDMA. The diameter setting for the measurements was the same as that of ambient particles (Sect. 2). The mean growth factors ($g_{f,m}$) of the AS particles under both dry and wet conditions were

retrieved using the same method as that for ambient particles (Sect. 3.1). The $g_{f,m}$ of the dry AS aerosol particles with diameters of 30–360 nm were 1.2–4.1 % deviated from unity (Table S2). The deviations were used to correct the difference of sizing between DMA1 and DMA2 for the g_f of AS and ambient aerosol particles measured at 85 % RH. The respective $g_{f,m}$ of AS particles at 85 % RH with d_{dry} of 30, 50, 70, 100, 200, 300, and 360 nm were 1.52, 1.54, 1.54, 1.54, 1.55, 1.57, and 1.59, which agree within 2.0 % with the calculated values ($g_{f,AS}$; Table S2) based on the Extended AIM Aerosol Thermodynamics Model II (E-AIM II, http://www.aim.env.uea.ac.uk/aim/model2/model2a.php; Clegg et al., 1998; Wexler and Clegg, 2002). The derivation of the hygroscopic growth factor of AS particles using the E-AIM II model is presented in Text S6.

Text S3. PMF analysis of organic mass spectra

The bulk mass spectra of organics observed in V-mode were subjected to PMF analysis (PMF Evaluation Tool v3.04A). For the analysis, high resolution fragment ions with signal to noise ratio (SNR) smaller than 0.2 were omitted, fragments with SNR in the range of 0.2–2 were down-weighted by a factor of three, and fragments related to CO2 (i.e., CO2, CO, H2O, HO, and O) were down-weighted so that fragment CO2 only contributed once. The obtained two-factor solution, with a more-oxygenated OA component (MOOA) and a less-oxygenated OA component (LOOA), with seed = 1 and fpeak = 0, was adopted for the explanation of OA composition. The two-factor PMF results are summarized in Fig. S1.

Text S4. Data screening methods

All the data except for the meteorological data obtained during the atmospheric observation were subjected to the screening to exclude data under possible influence from intermittent local anthropogenic emissions. For the SMPS data with 5 min resolution, and the BC and gaseous species data with 30 min resolution, if

the data value at one point was more than 30 % deviated from both the former data point and the next data point in the time series, the data at that time point was deleted. The chemical composition data derived from AMS measurements with 30 min resolution were deleted whenever the BC data were deleted. The hygroscopic growth data derived from the HTDMA measurements were deleted whenever the SMPS data were deleted. Furthermore, if the total count of particles measured using the CPC in the HTDMA in the diameter range of 0.80–2.2 times of d_{dry} (or 0.80–2.0 times of d_{dry} for particles with d_{dry} of 360 nm) during a single scan was less than eight, the HTDMA data was not used, either. Here, the d_{dry} were corrected for the difference of sizing between DMA1 and DMA2.

Text S5. Derivation of size-resolved volume fractions of the chemical components

The size-resolved volume fractions of inorganic salts (ε_i), organics (ε_{org}), and BC (ε_{BC}) were calculated as follows. First, BC was assumed to be internally mixed with non-refractory aerosol components and to have the same mass-size distribution as OA. The aerosol particles were assumed to be spherical and without voids. Using the PToF mode data from the AMS, the mass concentrations of aerosol components in the vacuum aerodynamic diameter (d_{va}) ranges that are ~1.0 (0.98–0.99) to 2.0 times of d_{dry} were obtained: the ranges of d_{va} for particles with d_{dry} of 100, 200, 300, and 360 nm were 98–197, 197–395, 295–589, and 353–707 nm, respectively. Second, the mole amounts of sulfate, nitrate, and ammonium in 1 m^3 of air were derived. Third, the amount of ammonium nitrate (AN), ammonium sulfate (AS), letovicite (LET), ammonium hydrogen sulfate (AHS), and sulfuric acid (SA) per mole in 1 m^3 of air was determined, assuming that nitrate was fully neutralized with ammonium, and that sulfate could present in the form of AS, LET, AHS, and/or SA according to the amount of remaining ammonium. The detected non-refractory chloride was not considered because of its low concentration compared with the concentrations of the other non-refractory components. The contribution of sea salt and minerals to the sub-micrometer aerosol

particles was likely small (Han et al., 2014; Deng et al., 2018) and was also not considered. Fourth, the volumes of BC, OA, and LET were derived using their respective densities and the volumes of AN, AS, AHS, and SA were derived using their respective molar volumes. The density of BC was assumed to be 1.77 g cm^{-3} (Park et al., 2004). The density of organics (ρ_{org}) was estimated to be 1.32 ± 0.09 g cm^{-3} using the O:C and H:C ratios of organics derived from AMS measurements (Kuwata et al., 2012), and the mean value of 1.32 g cm^{-3} was adopted for this study. The density of LET was assumed to be 1.83 g cm^{-3} (Padró et al., 2010). The molar volumes of AN, AS, AHS, and pure liquid SA, which are the same as the ones used in the E-AIM II model, were adopted in this study. Finally, the volume fractions of each species were obtained.

Text S6. Derivation of $g_{f,AS}$ and κ_i using the E-AIM II model

The hygroscopic growth factor of pure ammonium sulfate particles ($g_{f,AS}$) and the hygroscopicity parameter of each inorganic salt (κ_i) at 85 % RH were derived based on the output of the E-AIM II model and the κ–Köhler equation (Petters and Kreidenweis, 2007) as follows.

The water activity (a_w) range from 0.8000 to 0.8499 at a resolution of 0.0001 was applied to the E-AIM II model for unit mole of each inorganic salt at the temperature of 294 K. For the calculation, the partition of HNO_3, NH_3, and H_2SO_4 into the vapor phase was prevented and the formation of solid AS was also prevented. The hygroscopic growth factor (g_f) corresponding to each a_w was derived from the ratio of total wet volume (V_{wet}) to the dry molar volume of the pure salt. The κ_i corresponding to each a_w was derived from Equation 2 of Petters and Kreidenweis (2007). The exponential part of the κ–Köhler equation was derived on the assumption that the partial molar volume of water equals the molar volume of pure water. Here, a_w was calculated based on the relationship that the RH above the particle surface equals the product of the a_w and the exponential part of the κ–Köhler equation representing the Kelvin effect. For particles

with respective d_{dry}, an a_w value at which the RH above the particle surface was nearest to 85 % ($a_{w,85}$) was obtained by applying a wet diameter represented by the product of d_{dry} and g_f. The hygroscopicity parameter value at $a_{w,85}$ was defined as κ_i (Table S3). For AS, the g_f at $a_{w,85}$ was defined as $g_{f,AS}$ (Table S2). For the derivation of κ_i, the surface tension of the solution was applied, whereas for the derivation of κ_i (Sect. 3.1) the surface tension of pure water was applied. The uncertainty of the surface tension should not introduce large uncertainty in the derived κ_{org} because the difference of κ_i obtained using the surface tension of pure water and that obtained using the surface tension of the solution was small (within 0.38 %, Table S3).

Text S7. Determination of the range of d_{va} for the calculation of κ_{org}

The PToF mode AMS data over a lower d_{va} range was subjected to low signal intensity (Fig. S2) when it was adopted for the derivation of size-resolved κ_{org}. To determine the applicable range of d_{va} for this study, the mean mass-size distribution data of OA during the entire study period was compared to that of a baseline region (Fig. S3). The baseline region here is the transition region between the regions dominated by gaseous species and particle signals of OA, and corresponds to the PToF time region of 0.00135458–0.00150458 s. To eliminate data under the strong influence of the signals from gaseous species, the d_{va} of 98 nm (where the mass ratio of the mean observed OA to mean baseline OA became greater than three) was adopted as the lower limit of the d_{va} range for the deviation of κ_{org}. In Fig. S3, the mean mass-size distribution of OA for filtered air (collected by connecting a HEPA filter (TSI) to the inlet tubing outside the instrument room) is also presented for comparison. Only in the d_{va} range of 90–716 nm, the mean values of the observed OA mass in each d_{va} bin were greater than that of OA for the filtered air. This also indicates the strong influence of the signals from gaseous species at d_{va} smaller than ~90 nm. Because the OA data of filtered air was noisy, it was not used for the determination of the applicable d_{va} range.

Text S8. Derivation of size-resolved PMF factors

To explain the diurnal variation and size-dependence of κ_{org} from the compositional characteristics of OA, size-resolved PMF factors (LOOA and MOOA) were derived through multivariable linear regression analysis as follows.

First, the fragment profiles of LOOA and MOOA from bulk OA mass spectra were converted to the profiles in unit m/z resolution by summing up the intensity of the fragment ion signals at the same unit m/z. Then, for each time period in 2 h time resolution and for each PToF size bin *i*, the contributions from LOOA (a_i) and MOOA (b_i) were derived using the Solver function in Microsoft Excel by minimizing the value of the following formula:

$$\sum_{j=12}^{115} \left[x_{ij} - \left(a_i f_{1j} + b_i f_{2j}\right)\right]^2$$

Where x_{ij} is the measured signal intensity in size bin *i* at m/z = *j*, and f_{1j} and f_{2j} are the respective normalized signal intensity of LOOA and MOOA at m/z = *j*. The unit of x_{ij}, a_i, and b_i was μg m^{-3}, whereas f_{1j} and f_{2j} were dimensionless.

The size-resolved LOOA and MOOA were derived for the d_{va} range from ≤ 10 nm to around 900 nm (Fig. S6). However, only the d_{va} range above 98 nm was adopted for the analysis. This is because the uncertainty of the contributions from LOOA and MOOA in the lower d_{va} range was presumably relatively large, given the low organic signal intensity (Fig. S3) and high residual to measured OA mass ratio (Fig. S6).

Text S9. Assessment of the contributions of BSOA and anthropogenic OA to the enhancement of OA in the daytime

The contributions of BSOA and anthropogenic OA to the enhancement of OA in the daytime (in relation to the background period) were assessed using BC as a tracer of OA that did not come from BSOA

formation (non-BSOA-OA). Here, the non-BSOA-OA was considered the sum of regional OA and other anthropogenic OA. The diurnal variation data on the mass concentration of BC was scaled to represent the diurnal variation of non-BSOA-OA. For the scaling, the observed OA during the background period (i.e., 0600–0800 JST, when the daily minima of m_{org} appeared) was assumed to be composed only of non-BSOA-OA. The scaling factor was calculated to be 36.5. The mass concentrations of non-BSOA-OA ($m_{non\text{-}BSOA,bulk}$) and BSOA ($m_{BSOA,bulk}$) were then estimated using the following equations.

$$m_{non\text{-}BSOA,bulk} = m_{BC} \times 36.5 \quad \text{(S1)}$$

$$m_{BSOA,bulk} = m_{org} - m_{non\text{-}BSOA,bulk} \quad \text{(S2)}$$

Note that $m_{BSOA,bulk}$ and $m_{non\text{-}BSOA,bulk}$ are different from the mass concentrations of the BSOA and ROA defined from the size-resolved LOOA/MOOA data (Sect. 4.2.2 and Text S10). The $m_{BSOA,bulk}$ may be negatively biased because the charring of OA during the PSAP measurement may have resulted in a positive bias of m_{BC}. The increase of the OA mass concentration in the daytime ($m_{org,ENH}$) was estimated by subtracting the m_{org} during the background period from that during the period of interest. The ratio of $m_{BSOA,bulk}$ to $m_{org,ENH}$ was in the range 0.6–0.9 during 1200–1600 JST, and it was in the range 0.1–0.5 during 1600–2030 JST (Fig. S10). The result indicates that BSOA was the main contributor to the enhancement of OA at least during 1200–1600 JST. In a later period, a larger contribution from anthropogenic OA is not ruled out.

Text S10. Derivation of v_{BSOA} and v_{ROA} from v_{LOOA} and v_{MOOA}

Because the observed OA can be assumed to be contributed either by LOOA and MOOA, or by BSOA and ROA, the sum of LOOA and MOOA should equal the sum of BSOA and ROA. The size-resolved v_{BSOA} and v_{ROA} can be derived from the size-resolved v_{LOOA} and v_{MOOA}. From the analysis in Sect. 4.2.2, 0.97 (0.52), 0.88 (0.53), 0.80 (0.50), and 0.79 (0.45) of the volume of BSOA (ROA) for particles with d_{dry}

of 100, 200, 300, and 360 nm were assigned to LOOA, and the balances were assigned to MOOA. The relations are expressed by the equations:

$$v_{BSOA} + v_{ROA} = v_{LOOA} + v_{MOOA} \quad \text{(S3)}$$

$$a \times v_{BSOA} + b \times v_{ROA} = v_{LOOA} \quad \text{(S4)}$$

Where v_{BSOA}, v_{ROA}, v_{LOOA}, and v_{MOOA} are the size-resolved volume concentrations of BSOA, ROA, LOOA, and MOOA, respectively, and a and b represent the size-resolved volume fractions of BSOA and ROA, respectively, that were assigned to LOOA. The volume concentrations of BSOA and ROA were estimated using the equations:

$$v_{BSOA} = [(1 - b) / (a - b)] \times v_{LOOA} - [b / (a - b)] \times v_{MOOA} \quad \text{(S5)}$$

$$v_{ROA} = [(a - 1) / (a - b)] \times v_{MOOA} + [a / (a - b)] \times v_{LOOA} \quad \text{(S6)}$$

Equations (S5) and (S6) were used to estimate the contributions of BSOA to aerosol water uptake and to the CCN number concentration (Sect. 4.4 and Text S11).

Text S11. Estimation of the contributions of OA and BSOA to CCN concentrations

The contributions of OA and BSOA to the CCN number concentration were estimated from their size-resolved fractional contributions to aerosol water uptake and from the measured aerosol number-size distributions. The analysis was performed for diurnal variation data with 2 h resolution. A schematic of the estimate is presented in Fig. S17. For the estimate, the observed aerosol particles were assumed to be internally mixed, and the CCN activation diameters (d_{act}) under the condition of 0.4 % SS were derived using the reconstructed hygroscopicity parameters ($\kappa_{t,reconst,org}$ and $\kappa_{t,reconst,BSOA}$ for the analysis of the contributions of OA and BSOA, respectively). For the calculation of d_{act}, κ-Köhler theory was applied in the manner of Deng et al. (2018). The contributions of OA (BSOA) to the water uptake of particles with d_{dry} of 100, 200, 300, and 360 nm were applied for the diameter ranges of d_{act}–150, 150–250, 250–330,

Deleted: all the particles with d_{dry} larger than 70 nm

Deleted: were assumed to be CCN active.

Deleted: 70

330–430 nm, respectively. For the diameter ranges larger than 430 nm, the CCN number concentration contributed by OA (BSOA) was not considered because of the low aerosol number concentrations. In each diameter range, the fractional contribution of OA (BSOA) to $dN_{CN}/d\log d_{dry}$ equals the fractional contribution of OA (BSOA) to the total aerosol water uptake, which was represented as the product of the volume fraction of OA (BSOA) and κ_{org} (κ_{BSOA}) divided by κ_i [i.e., $\varepsilon_{org}\kappa_{org}/\kappa_i$ ($\varepsilon_{BSOA}\kappa_{BSOA}/\kappa_i$)]. The total fractional contribution of OA (BSOA) to the total CCN number concentration, $F_{CCN,OA}$ ($F_{CCN,BSOA}$), equals the integration of the product of the water uptake fraction and $dN_{CN}/d\log d_{dry}$ above the assumed CCN activation diameter (70 nm), divided by the total CCN number concentration.

For the above analysis, the water uptake of each aerosol component was represented by the product of the volume fraction of the aerosol component (ε_i) and its hygroscopicity (κ_i), that is, $\varepsilon_i\kappa_i$. The mean ε_i in each 2 h time section of the day was derived as follows. First, the mean values of the volume concentrations of each inorganic species, organics, and organic fractions (AN, AS, LET, AHS, SA, BC, OA, LOOA, and MOOA; $\bar{v}_i$) were calculated from the 2 h resolution data. Second, the mean volume concentrations of LOOA ($\bar{v}_{LOOA}$) and MOOA ($\bar{v}_{MOOA}$) were scaled so that their sum equals the mean volume concentration of OA ($\bar{v}_{OA}$). Third, the mean volume concentrations of BSOA ($\bar{v}_{BSOA}$) and ROA ($\bar{v}_{ROA}$) were estimated using Eqs. (S5) and (S6). Then, ε_i was calculated directly from those $\bar{v}_i$. The κ of the inorganic salts under the condition of 0.4 % SS, and at the temperature of the HTDMA measurement in this study, were used to consider the difference of κ between sub- and super-saturated water vapor conditions. Here, the κ for AN, AS, LET, AHS, and SA were calculated to be 0.72, 0.59, 0.62, 0.61, and 0.65, respectively, following the method in Deng et al. (2018). The difference of the κ of organics under sub- and super-saturated conditions was not considered. The κ values of OA and BSOA used for the calculation are presented in Tables S10 and S11, respectively. The contributions of OA and BSOA to the water uptake were calculated as $\varepsilon_{org}\kappa_{org}/\kappa_{i,reconst,org}$ and $\varepsilon_{BSOA}\kappa_{BSOA}/\kappa_{i,reconst,BSOA}$, respectively, where,

Deleted: 42

Deleted: 73

Deleted: 60, 0.63

$$\kappa_{t,reconst,org} = \varepsilon_{AN}\kappa_{AN} + \varepsilon_{AS}\kappa_{AS} + \varepsilon_{LET}\kappa_{LET} + \varepsilon_{AHS}\kappa_{AHS} + \varepsilon_{SA}\kappa_{SA} + \varepsilon_{org}\kappa_{org} \quad \text{(S7)}$$

$$\kappa_{t,reconst,BSOA} = \varepsilon_{AN}\kappa_{AN} + \varepsilon_{AS}\kappa_{AS} + \varepsilon_{LET}\kappa_{LET} + \varepsilon_{AHS}\kappa_{AHS} + \varepsilon_{SA}\kappa_{SA} + \varepsilon_{BSOA}\kappa_{BSOA} + \varepsilon_{ROA}\kappa_{ROA} \quad \text{(S8)}$$

References:

Clegg, S. L., Brimblecombe, P., and Wexler, A. S.: Thermodynamic model of the system H+-NH4+-SO42−-NO3−-H2O at tropospheric temperatures, Journal of Physical Chemistry A, 102, 2137-2154, 10.1021/jp973042r, 1998.

Deng, Y. G., Kagami, S., Ogawa, S., Kawana, K., Nakayama, T., Kubodera, R., Adachi, K., Hussein, T., Miyazaki, Y., and Mochida, M.: Hygroscopicity of Organic Aerosols and Their Contributions to CCN Concentrations Over a Midlatitude Forest in Japan, Journal of Geophysical Research-Atmospheres, 123, 9703-9723, 10.1029/2017jd027292, 2018.

Draxier, R. R., and Hess, G. D.: An overview of the HYSPLIT_4 modelling system for trajectories, dispersion and deposition, Australian Meteorological Magazine, 47, 295-308, 1998.

Han, Y. M., Iwamoto, Y., Nakayama, T., Kawamura, K., and Mochida, M.: Formation and evolution of biogenic secondary organic aerosol over a forest site in Japan, Journal of Geophysical Research-Atmospheres, 119, 259-273, 10.1002/2013jd020390, 2014.

Kawana, K., Kuba, N., and Mochida, M.: Assessment of cloud condensation nucleus activation of urban aerosol particles with different hygroscopicity and the application to the cloud parcel model, Journal of Geophysical Research-Atmospheres, 119, 3352-3371, 10.1002/2013jd020827, 2014.

Kuwata, M., Zorn, S. R., and Martin, S. T.: Using Elemental Ratios to Predict the Density of Organic Material Composed of Carbon, Hydrogen, and Oxygen, Environmental Science & Technology, 46, 787-794, 10.1021/es202525q, 2012.

Padro, L. T., Tkacik, D., Lathem, T., Hennigan, C. J., Sullivan, A. P., Weber, R. J., Huey, L. G., and Nenes, A.: Investigation of cloud condensation nuclei properties and droplet growth kinetics of the water-soluble aerosol fraction in Mexico City, Journal of Geophysical Research-Atmospheres, 115, 13, 10.1029/2009jd013195, 2010.

Park, K., Kittelson, D. B., Zachariah, M. R., and McMurry, P. H.: Measurement of inherent material density of nanoparticle agglomerates, Journal of Nanoparticle Research, 6, 267-272, 10.1023/B:NANO.0000034657.71309.e6, 2004.

Petters, M. D., and Kreidenweis, S. M.: A single parameter representation of hygroscopic growth and cloud condensation nucleus activity, Atmospheric Chemistry and Physics, 7, 1961-1971, 10.5194/acp-7-1961-2007, 2007.

Deleted: **Text S12. Assessment of the diurnal variation of the CCN activation diameter**
Although the variation of the CCN activation diameter with time influences the prediction of $F_{CCN,OA}$ and $F_{CCN,BSOA}$, the degree was found to be small. In the summertime observation in 2014 (Deng et al., 2018), the range of the diurnal variation of the CCN activation diameter was from 64 to 76 nm, whereas the CCN activation diameter assumed in this study is 70 nm. Applying 64 or 76 nm to an assumed CCN activation diameter results in the deviations of the predicted $F_{CCN,OA}$ and $F_{CCN,BSOA}$ only by −1.9–2.3 % and −3.1–3.8 %, respectively.

Text S13. Assessment of the change of CCN activation diameter accompanying the aging of BSOA
The aging of BSOA may change the CCN activation diameter and influence the prediction of $F_{CCN,BSOA}$. However, the change and the influence are considered to be small as explained below. If the range of κ_i of 0.17 to 0.35 (i.e., the κ_i range of (mean – SD) to (mean + SD) under 0.42 % SS condition in Deng et al. (2018)), and the approximate maximum ε_{BSOA} of 0.6 (Fig. S18) are applied, the increase of κ_{BSOA} by 0.09 (i.e., the difference between κ_{BSOA} and κ_{ROA} for particles with d_{dry} of 100 nm) leads to a decrease in the CCN activation diameter by 3–7 nm. The resulting decrease leads to increase of the predicted $F_{CCN,BSOA}$ by 0.15–3.8 %, which is regarded as small.

Wexler, A. S., and Clegg, S. L.: Atmospheric aerosol models for systems including the ions H+, NH4+, Na+, SO42−, NO3−,Cl−, Br−, and H2O, Journal of Geophysical Research-Atmospheres, 107, 14, 10.1029/2001jd000451, 2002.

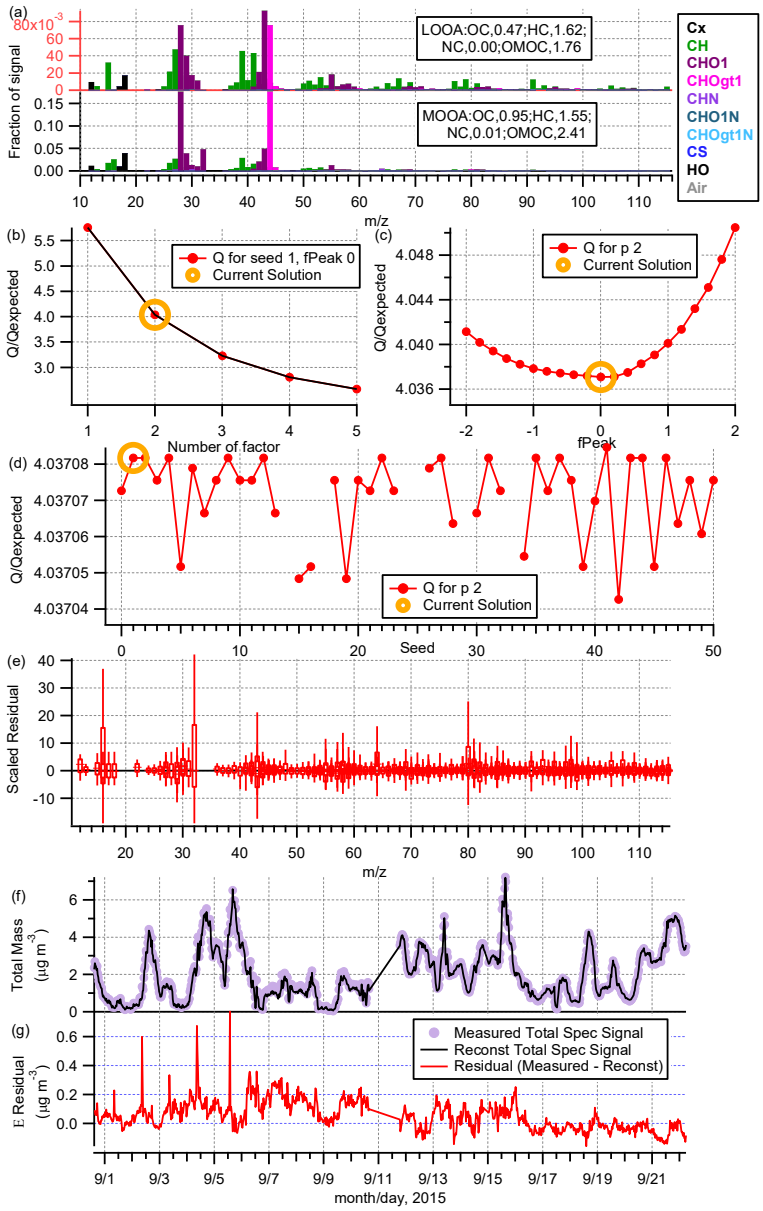
(a)
Fraction of signal
LOOA:OC,0.47;HC,1.62;
NC,0.00;OMOC,1.76
MOOA:OC,0.95;HC,1.55;
NC,0.01;OMOC,2.41
Cx
CH
CHO1
CHOgt1
CHN
CHO1N
CHOgt1N
CS
HO
Air
m/z
(b)
Q/Qexpected
Q for seed 1, fPeak 0
Current Solution
(c)
Q for p 2
Current Solution
fPeak
(d)
Number of factor
Q for p 2
Current Solution
Seed
(e)
Scaled Residual
m/z
(f)
Total Mass (µg m-3)
(g)
E Residual (µg m-3)
Measured Total Spec Signal
Reconst Total Spec Signal
Residual (Measured - Reconst)
9/1
9/3
9/5
9/7
9/9
9/11
9/13
9/15
9/17
9/19
9/21
month/day, 2015

Figure S1: Summary of the two-factor result from the PMF analysis: (a) organic mass spectra of LOOA and MOOA colored according to ion groups (fpeak = 0 and SEED = 1), and the atomic ratios of O to C, H to C, and N to C, as well as OM to OC ratio for each factor; (b) Q/Qexpected as a function of the number of factors, where Q is the sum of the weighted squared residuals and Qexpected is the expected Q value; (c) Q/Qexpected as a function of the fpeak values with SEED = 1 and the number of factor = 2; (d) Q/Qexpected as a function of the SEED values with fpeak = 0 and the number of factor = 2; (e) distributions of the scaled residual for each m/z (fpeak = 0 and SEED = 1); time series of (f) the measured organic mass concentrations and those reconstructed (= LOOA + MOOA) (fpeak = 0 and SEED = 1), and (g) residual OA (= measured − reconstructed) (fpeak = 0 and SEED = 1).

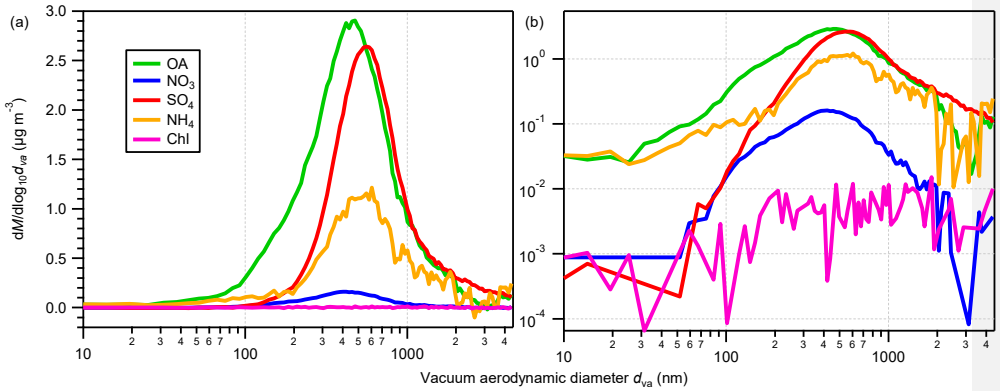

Figure S2: Mean mass-size distributions of organics (OA), sulfate (SO_4), ammonium (NH_4), nitrate (NO_3), and chloride (Chl) in (a) linear and (b) logarithmic scales over the entire study period.

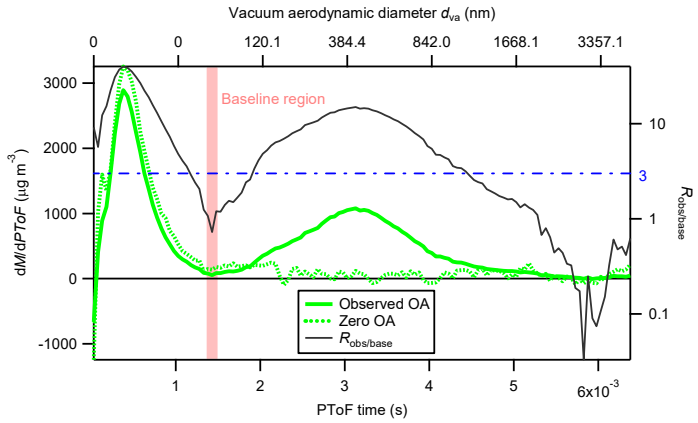

Figure S3: d*M*/d*PToF* (*M* and *PToF* here refer to mass concentration and PToF time, respectively) versus PToF time for the observed OA and OA measured by placing a HEPA filter in the inlet tubing outside the instrument room (zero OA), averaged for the entire study period. The region shaded in pink indicates the PToF time region chosen as a baseline for evaluation of the effective PToF diameter range. (Note that this is not the DC marker region.) The dark solid curve is the absolute value of the ratio of the observed OA at respective PToF time to the mean of the observed OA in the baseline region ($R_{obs/base}$). The blue dash-dotted line indicates the $R_{obs/base}$ value of three. The vacuum aerodynamic diameter that corresponds to the PToF time is presented on the top axis.

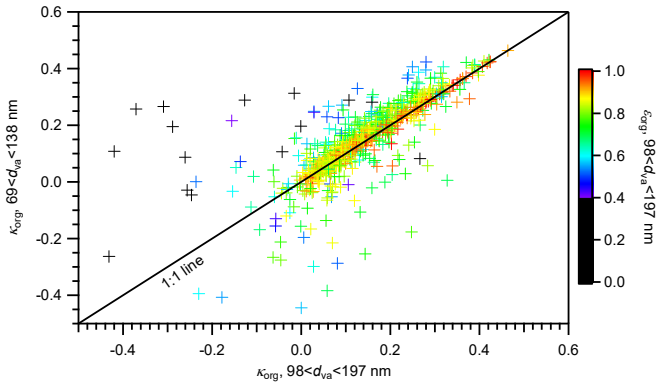

Figure S4: κ_{org} of 100 nm particles derived based on the chemical composition in the vacuum aerodynamic diameter (d_{va}) range of 69–138 nm versus that of 98–197 nm. Data points with κ_{org} smaller than −0.50 or κ_{org} higher than 0.60 are not presented.

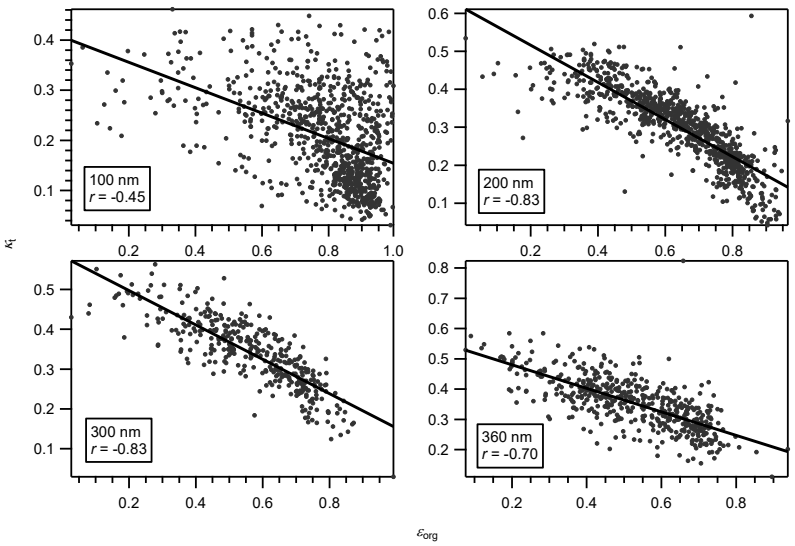

Figure S5: κ_t versus ε_{org} for particles with d_{dry} of 100, 200, 300, and 360 nm for the entire study period. In each panel, marks and a solid line represent individual data and the corresponding linear regression line, respectively. The correlation coefficient (r) of each is also presented.

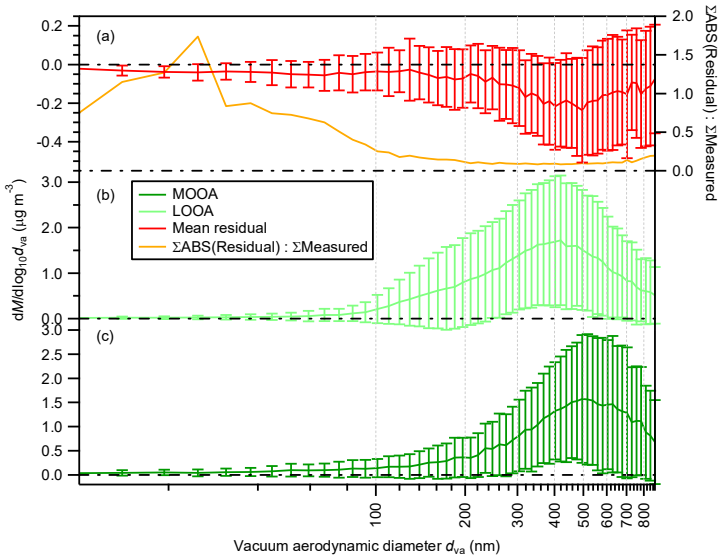

Figure S6: Mean mass-size distributions of (a) residual, (b) LOOA, and (c) MOOA over the entire study period. The residual is the difference between the measured and reconstructed (i.e., LOOA + MOOA) mass concentrations of OA in each size bin. The error bars indicate the standard deviation. The ratios of the sum of the absolute value of the residual to the measured mass concentration of OA are superimposed in panel (a) (right axis).

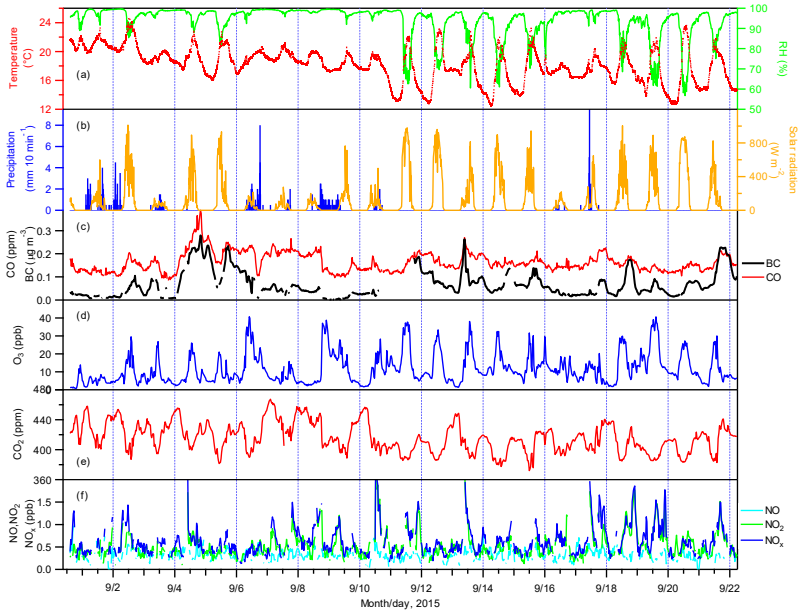

Figure S7: Time series of (a) air temperature and relative humidity (RH), (b) precipitation and solar radiation, (c) mass concentration of BC, and mixing ratios of (c) CO, (d) O_3, (e) CO_2, and (f) NO, NO_2, and NO_x.

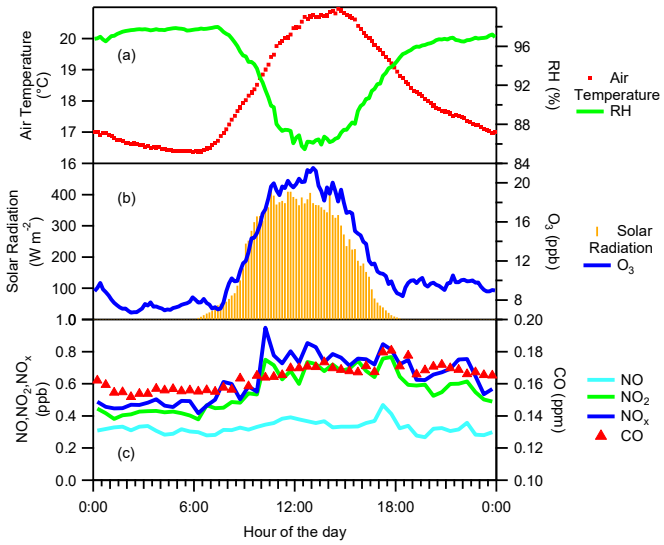

Figure S8: Diurnal variations of (a) air temperature and relative humidity (RH), (b) solar radiation and the mixing ratios of O_3, and (c) mixing ratios of NO, NO_2, NO_x, and CO over the entire study period.

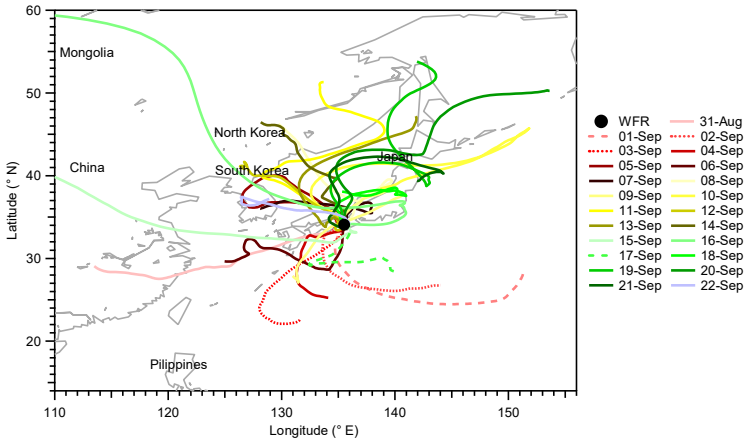

Figure S9: Five-day backward air mass trajectories from 500 m agl (above ground level) over Wakayama Forest Research Station at one-day intervals. The arrival time of the air masses at the study site was 1500 JST. The solid circle denotes the location of the study site. Solid trajectories are for days when more than 22 of the 24 hourly trajectories are from terrestrial regions. Dashed trajectories are for days when more

than 21 of the 24 hourly trajectories are from the North Pacific. Dotted trajectories are for days when 10 of the 24 hourly trajectories are from the North Pacific. The map is based on GSHHG 2.3.4; the shoreline polygon data at crude resolution is used. We consider an air mass is from the North Pacific if the trajectory never passes over terrestrial area that appears on the map before it reaches the Kii Peninsula. The trajectories were produced using NOAA's HYSPLIT atmospheric transport and dispersion modeling system (Draxler and Hess, 1998).

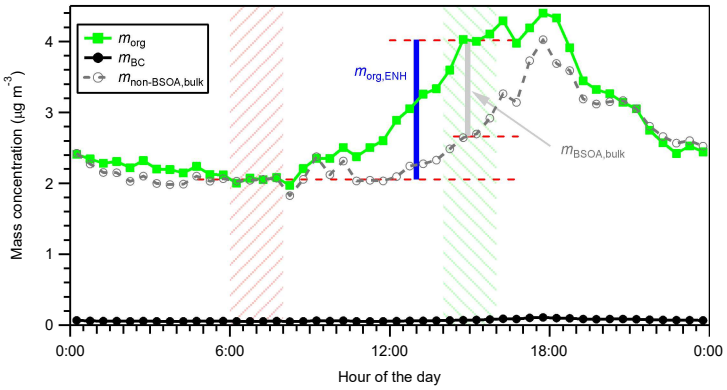

Figure S10. Diurnal variation of the mass concentrations of OA (m_{org}), BC (m_{BC}), and non-BSOA-OA ($m_{non\text{-}BSOA,bulk}$; Text S9) during the entire study period. The left-slash pattern represents the background period. As an example, the vertical bars represent the estimates of the total enhancement of OA ($m_{org,ENH}$; blue) and the enhancement contributed by BSOA ($m_{BSOA,bulk}$; gray) for the period 1400–1600 JST (right slash pattern).

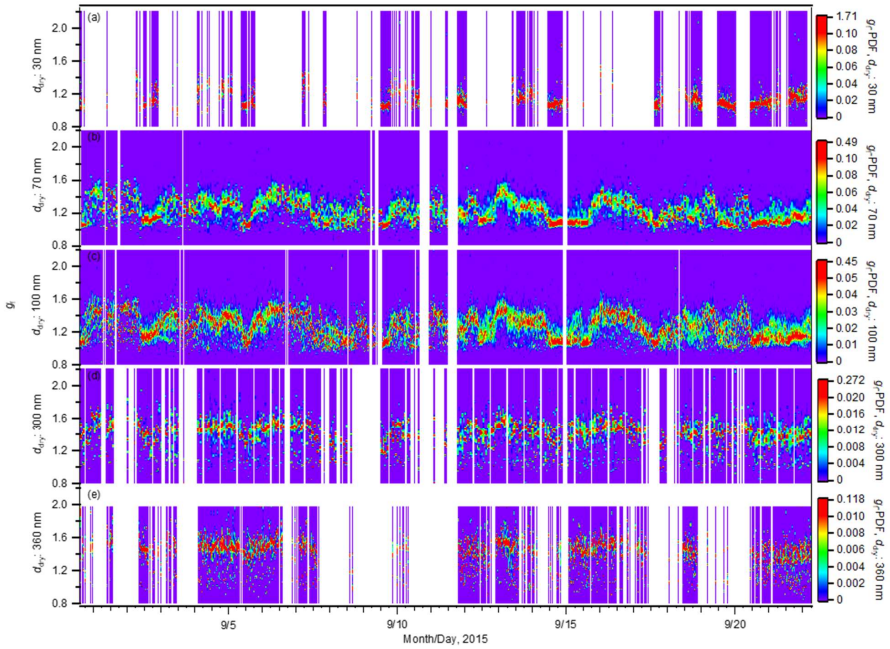

Figure S11: Time series of the probability distribution functions of the hygroscopic growth factors (g_f-PDF) of aerosol particles with d_{dry} of (a) 30, (b) 70, (c) 100, (d) 300, and (e) 360 nm.

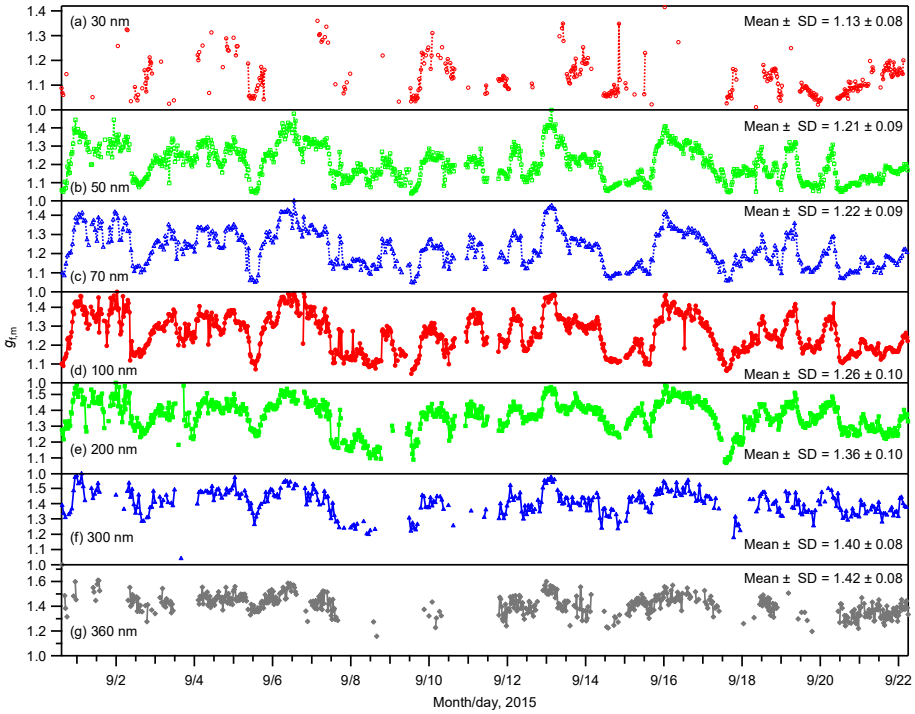

Figure S12: Time series of the mean growth factors ($g_{f,m}$) of aerosol particles with different dry diameters. The mean ± SD values over the entire study period for each diameter are also presented.

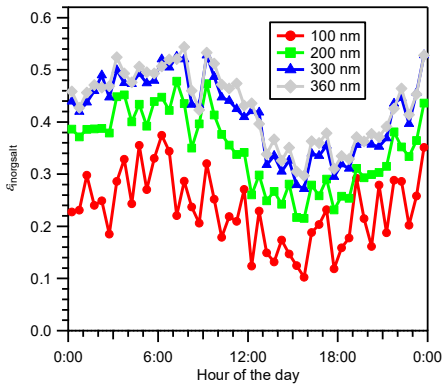

Figure S13: Diurnal variation of the size-resolved volume fractions of total inorganic salts ($\varepsilon_{inorgsalt}$) during the entire study period.

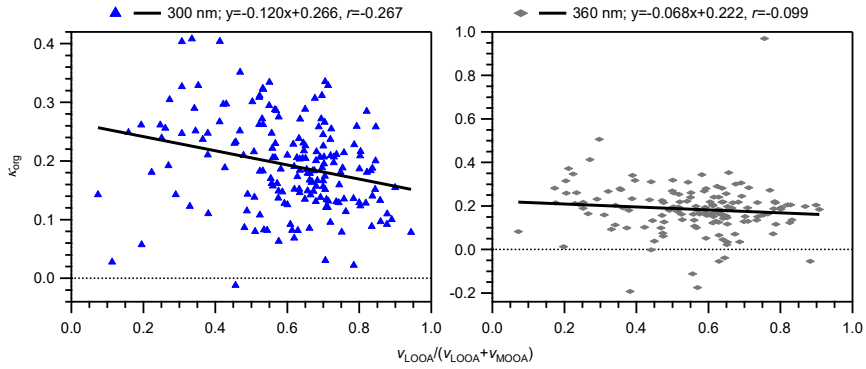

Figure S14: The κ_{org} versus $v_{LOOA}/(v_{LOOA}+v_{MOOA})$ for particles with d_{dry} of 300 and 360 nm. The time resolution of the data is 2 h. In each panel, marks and a solid line represent individual data and the corresponding linear regression line, respectively. The regression equation and correlation coefficient of each are also presented. Only data with ε_{org} greater than 0.40 are used.

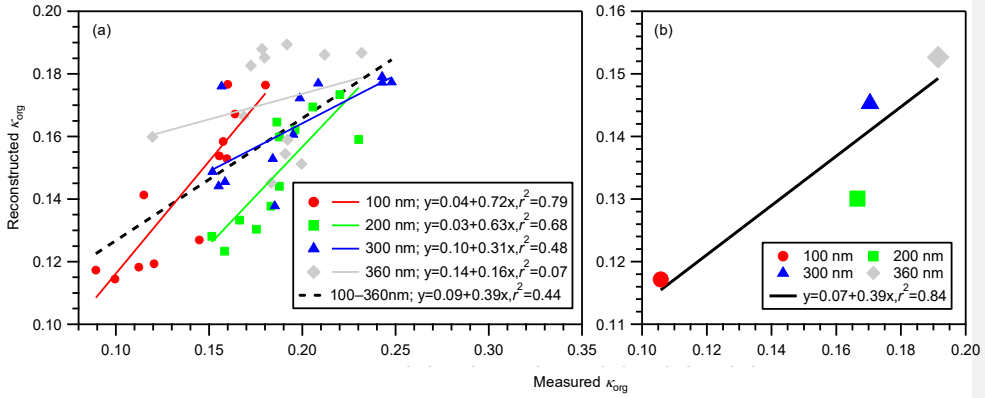

Figure S15: The κ_{org} reconstructed using κ_{LOOA}, κ_{MOOA}, and size-resolved $v_{LOOA}/(v_{LOOA}+v_{MOOA})$ (reconstructed κ_{org}) versus the κ_{org} derived from measured κ_i and aerosol chemical composition (measured κ_{org}; Sect. 3.2). In panel (a), markers represent size-resolved diurnal variation data at 2 h resolution, solid lines are linear regression lines for particles with respective diameters, and the dashed line is the linear regression line for all 100–360 nm particles. In panel (b), markers represent the size-resolved mean κ_{org} during 1200–2000 JST, and the solid line is the linear regression line for the size-resolved mean κ_{org}. Respective regression equations and coefficients of determination (r^2) are also presented. Only κ_{org} data with ε_{org} greater than 0.40 are used for the comparison.

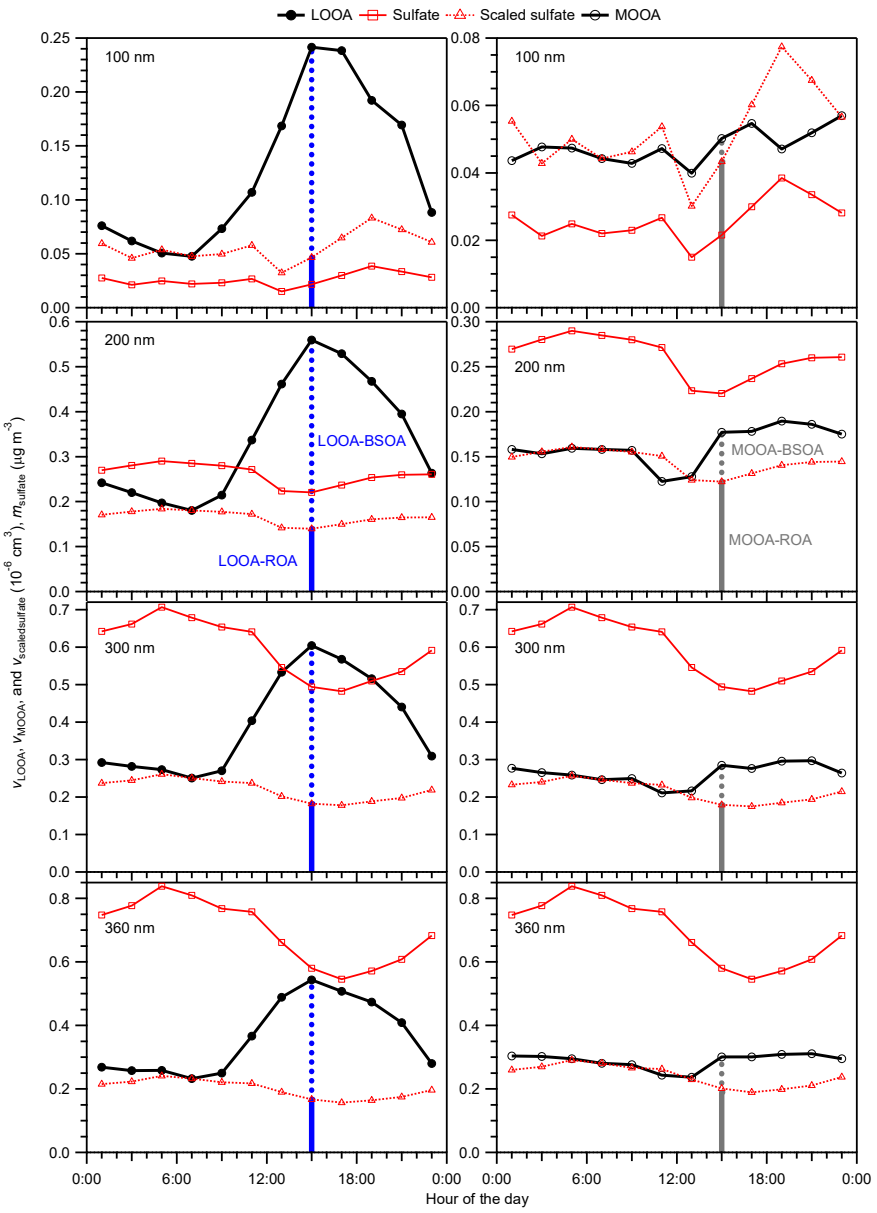
LOOA
Sulfate
Scaled sulfate
MOOA
100 nm
200 nm
300 nm
360 nm
LOOA-BSOA
LOOA-ROA
MOOA-BSOA
MOOA-ROA
v_{LOOA}, v_{MOOA}, and $v_{scaledsulfate}$ (10^{-6} cm^3), $m_{sulfate}$ (μg m^{-3})
Hour of the day
0:00
6:00
12:00
18:00

Figure S16: Diurnal variation of the volume concentrations of LOOA and MOOA and the mass concentration of sulfate for particles with d_{dry} of 100, 200, 300, and 360 nm over the entire study period. The scaled sulfate represents the diurnal variation of ROA that was contributed by LOOA (left panels) or MOOA (right panels). The scaling factor for the scaled sulfate in each panel is the mean volume concentration of OA during 0600–0800 JST, divided by the mean mass concentration of sulfate in the same period. The volume concentrations of LOOA and MOOA were derived from the respective mass concentrations (Text S8). The densities of LOOA and MOOA were calculated using their O:C and H:C ratios following Kuwata et al. (2012) and were 1.24 and 1.54 g cm^{-3}, respectively.

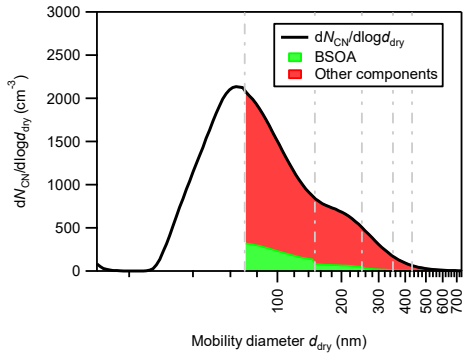

Figure S17: Estimate of the contributions of BSOA to the CCN number concentration from the viewpoint of its size-resolved contribution to the aerosol water uptake. The solid line indicates the mean aerosol number-size distribution during the entire study period. Shaded areas in green represent the fraction of CCN contributed by BSOA and in red, that contributed by other components assuming a CCN activation diameter of 70 nm (Text S11).

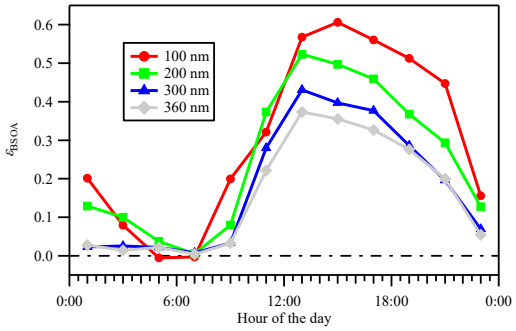

Figure S18: The diurnal variation of the volume fractions of BSOA (ε_{BSOA}) for particles with d_{dry} of 100, 200, 300, and 360 nm over the entire study period (Text S11).

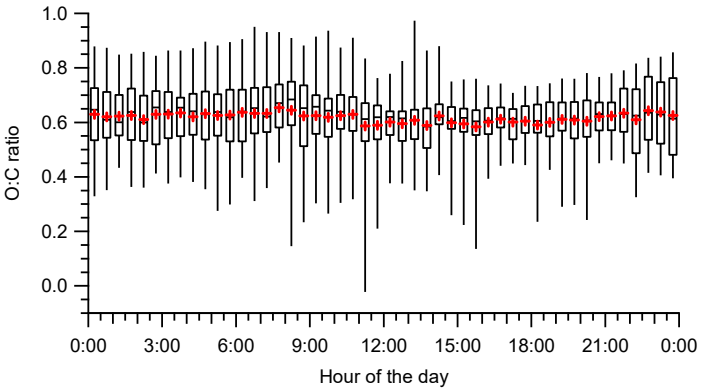

Figure S19: Box and whiskers plot of the diurnal variation of the O:C ratios of bulk OA (only data with $m_{org} > 0.3$ μg m^{-3} are included) for the entire study period. The horizontal lines in the boxes indicate the median values, boundaries of the boxes indicate the 25th- and 75th-percentiles, and the whiskers indicate the highest and lowest values. The cross symbols in the boxes indicate the mean values.

Table S1: Mode diameters [a] of PSL size standards measured by DMAs in the HTDMA (DMA1 and DMA2) and the SMPS (DMA3) (mean ± SD, nm)

Manufacturer	DMA1		DMA2		DMA3	
warranty	Before [c]	After [d]	Before [c]	After [d]	Before [c]	After [d]
55 (± 1) [b]	56.6 ± 0.4	56.2 ± 0.4	56.8 ± 0.4	-	59.9 ± 0.2	-
100 (± 3) [b]	98.0 ± 0.2	98.4 ± 0.1	97.0 ± 0.1	96.2 ± 0.2	101.2 ± 0.3	101.1 ± 0.1
309 (± 9) [b]	297.7 ± 0.8	298.0 ± 0.4	290.4 ± 1.2	-	303.6 ± 0.3	-
498 (± 9) [b]	-	-	478.4 ± 5.8	-	499.6 ± 4.4	-

[a] The mean ± SD of the mode diameters from fittings are presented (unit: nm).
[b] Mean diameter (± the expanded uncertainty; $k = 2$).
[c] Before the atmospheric observations.
[d] After the atmospheric observations.

Table S2: The $g_{f,m}$ of ammonium sulfate (AS) particles measured under dry condition ($g_{f,m,dryAS}$) and at 85 % RH ($g_{f,m,wetAS}$), and calculated g_f of AS particles at 85 % RH ($g_{f,AS}$)

d_{dry} (nm)	30	50	70	100	200	300	360
$g_{f,m,dryAS}$	0.959	0.976	0.984	0.985	0.988	0.982	0.981
$g_{f,m,wetAS}$[a]	1.52	1.54	1.54	1.54	1.55	1.57	1.59

$g_{f,AS}$[a]	1.49	1.52	1.54	1.55	1.57	1.57	1.57
Difference (%)[b]	2.0	1.3	0	–0.65	–1.3	0	1.3

[a] Corrected for the difference of sizing between DMA1 and DMA2.
[b] $((g_{f,m,wetAS} - g_{f,AS}) / g_{f,AS}) \times 100$.

Table S3: The κ values of inorganic salts (κ_i) at 85 % RH derived using the surface tension of the solution and of pure water

	κ_i, with surface tension of solution				κ_i, with surface tension of pure water			
d_{dry} (nm)	**100**	**200**	**300**	**360**	**100**	**200**	**300**	**360**
AN	0.553	0.555	0.555	0.556	0.553	0.555	0.556	0.556
AS	0.533	0.527	0.525	0.524	0.531	0.526	0.524	0.524
LET	0.550	0.545	0.543	0.543	0.549	0.544	0.543	0.543
AHS	0.612	0.607	0.605	0.605	0.612	0.607	0.605	0.605
SA	0.972	0.959	0.955	0.953	0.971	0.959	0.955	0.953

Table S4: Data in Fig. 3 of the main manuscript ("DataInFigure3ofTheManuscript.xlsx").

Table S5: Data in Fig. 4 of the main manuscript ("DataInFigure4ofTheManuscript.xlsx").

Table S6: Data in Fig. 5 of the main manuscript ("DataInFigure5ofTheManuscript.xlsx").

Table S7: Comparisons of κ_{org} and $v_{LOOA}/(v_{LOOA}+v_{MOOA})$ between particles with different d_{dry}

d_{dry} of particles to compare (nm)	1200–2000 JST				2000–1200 JST			
	κ_{org}		$v_{LOOA}/(v_{LOOA}+v_{MOOA})$		κ_{org}		$v_{LOOA}/(v_{LOOA}+v_{MOOA})$	
	Diff[a]	**p-value**[c]	**Diff**[b]	**p-value**[c]	**Diff**[a]	**p-value**[c]	**Diff**[b]	**p-value**[c]
200 vs 100	0.06	<0.01	–0.06	0.02	0.04	<0.01	–0.01	0.65
300 vs 200	<0.01	0.71	–0.08	<0.01	<0.01	0.31	–0.06	<0.01
360 vs 300	0.02	0.15	–0.04	<0.01	–0.02	0.02	–0.05	<0.01
360 vs 200	0.02	0.07	–0.11	<0.01	–0.02	0.07	–0.11	<0.01

[a] The mean of (the κ_{org} of particles with relatively large d_{dry} – the κ_{org} of particles with relatively small d_{dry}).
[b] The mean of (the $v_{LOOA}/(v_{LOOA}+v_{MOOA})$ of particles with relatively large d_{dry} – the $v_{LOOA}/(v_{LOOA}+v_{MOOA})$ of particles with relatively small d_{dry}).
[c] From 10 % two-sided t-test for the significance of the difference of Diff from zero. Low values indicate significant differences.

Table S8: Diurnal variation of κ_i and κ_{org} at 2 h resolution, and their mean and SD for the entire period

	κ_i							κ_{org}			
d_{dry} (nm)	**30**	**50**	**70**	**100**	**200**	**300**	**360**	**100**	**200**	**300**	**360**
0000–0200 JST	0.16	0.20	0.22	0.24	0.34	0.37	0.36	0.16	0.23	0.25	0.21
0200–0400 JST	0.22	0.21	0.22	0.24	0.34	0.37	0.35	0.16	0.20	0.21	0.18

0400–0600 JST	0.18	0.21	0.22	0.25	0.34	0.38	0.39	0.16	0.21	0.24	0.23
0600–0800 JST	0.21	0.22	0.21	0.25	0.35	0.38	0.36	0.18	0.22	0.24	0.19
0800–1000 JST	0.15	0.18	0.21	0.22	0.32	0.33	0.37	0.16	0.19	0.16	0.18
1000–1200 JST	0.13	0.16	0.16	0.19	0.29	0.33	0.34	0.12	0.17	0.15	0.12
1200–1400 JST	0.090	0.14	0.14	0.16	0.26	0.32	0.34	0.11	0.16	0.19	0.18
1400–1600 JST	0.083	0.13	0.13	0.16	0.24	0.28	0.33	0.10	0.15	0.16	0.20
1600–1800 JST	0.10	0.14	0.14	0.17	0.25	0.28	0.32	0.089	0.18	0.16	0.19
1800–2000 JST	0.13	0.15	0.16	0.19	0.27	0.31	0.32	0.12	0.18	0.18	0.19
2000–2200 JST	0.14	0.18	0.18	0.21	0.29	0.33	0.34	0.14	0.19	0.20	0.17
2200–0000 JST	0.12	0.19	0.20	0.23	0.31	0.35	0.36	0.16	0.19	0.20	0.17
Mean for entire period	0.12	0.18	0.18	0.21	0.30	0.34	0.35	0.13	0.18	0.19	0.19
SD for entire period	0.079	0.090	0.089	0.094	0.10	0.087	0.086	0.11	0.085	0.084	0.11

Table S9: Data in Fig. 6 of the main manuscript.

Hour of the day	$F_{CCN,OA}$ (%)	$F_{CCN,BSOA}$ (%; fresh BSOA)	$F_{CCN,BSOA}$ (%; aged BSOA)
0000–0200 JST	44.7	5.81	10.6
0200–0400 JST	44.9	2.67	4.89
0400–0600 JST	40.4	0.249	0.356
0600–0800 JST	43.2	-3.63×10^{-3}	-0.0326
0800–1000 JST	44.3	5.50	10.1
1000–1200 JST	42.0	12.7	21.3
1200–1400 JST	51.8	25.8	39.4
1400–1600 JST	51.7	27.8	42.2
1600–1800 JST	47.0	24.5	38.2
1800–2000 JST	45.8	19.6	31.8
2000–2200 JST	49.4	16.3	27.3
2200–0000 JST	45.4	4.99	9.09

Formatted ... [1]
Deleted: 5
Deleted: 85
Formatted ... [4]
Formatted ... [2]
Formatted Table ... [3]
Deleted: 66
Deleted: 88
Formatted ... [6]
Formatted ... [5]
Formatted ... [8]
Deleted: 1
Deleted: 238
Deleted: 338
Formatted ... [7]
Deleted: 42.8
Formatted ... [10]
Deleted: −6.41
Formatted ... [11]
Deleted: −….0.0373
Formatted ... [12]
Formatted ... [9]
Formatted ... [14]
Deleted: 5
Deleted: 62
Deleted: 3
Formatted ... [13]
Formatted ... [16]
Deleted: 7
Formatted ... [15]
Deleted: 53.0
Formatted ... [18]
Deleted: 26.2
Deleted: 8
Formatted ... [17]
Deleted: 52
Formatted ... [20]
Deleted: 28.4
Deleted: 6
Formatted ... [19]
Formatted ... [22]
Deleted: 3
Deleted: 9
Deleted: 5
Formatted ... [21]
Formatted ... [24]
Deleted: 7
Deleted: 8
Deleted: 9
Formatted ... [23]
Formatted ... [26]
Deleted: 6
Deleted: 5
Formatted ... [25]
Formatted ... [28]
Deleted: 3
Deleted: 10
Formatted ... [27]

Table S10: Different assumptions of κ_{org} for the prediction of $F_{CCN,OA}$

	TimeSize κ_{org}[a]				SizeReso κ_{org}[b]				TimeReso κ_{org}[c]				Single κ_{org}[d]			
d_{dry} (nm)	**100**	**200**	**300**	**360**	**100**	**200**	**300**	**360**	**100**	**200**	**300**	**360**	**100**	**200**	**300**	**360**
0000–0200 JST	0.16	0.23	0.25	0.21						0.21						
0200–0400 JST	0.16	0.20	0.21	0.18						0.19						
0400–0600 JST	0.16	0.21	0.24	0.23						0.21						
0600–0800 JST	0.18	0.22	0.24	0.19						0.21						
0800–1000 JST	0.16	0.19	0.16	0.18						0.17						
1000–1200 JST	0.12	0.17	0.15	0.12	0.14	0.19	0.19	0.19		0.14				0.18		
1200–1400 JST	0.11	0.16	0.19	0.18						0.16						
1400–1600 JST	0.10	0.15	0.16	0.20						0.15						
1600–1800 JST	0.089	0.18	0.16	0.19						0.15						
1800–2000 JST	0.12	0.18	0.18	0.19						0.17						
2000–2200 JST	0.14	0.19	0.20	0.17						0.17						
2200–0000 JST	0.16	0.19	0.20	0.17						0.18						

[a] Time- and size-resolved κ_{org}.
[b] Time-averaged, size-resolved κ_{org}.
[c] Time-resolved, size-averaged κ_{org}.
[d] Time- and size-averaged κ_{org}.

Table S11: Different assumptions of κ_{BSOA} for the prediction of $F_{CCN,BSOA}$

d_{dry} (nm)	Size-resolved κ_{BSOA}	Size-averaged κ_{BSOA}	Aged, size-resolved κ_{BSOA}
100	0.089	0.11	0.18
200	0.11		0.18
300	0.12		0.18
360	0.12		0.19

Table S12: Data in Fig. 7 of the main manuscript.

Hour of day	Ratios of different $F_{CCN,OA}$				Ratios of different $F_{CCN,BSOA}$		
	TimeSize κ_{org}[a]	SizeReso κ_{org}[b]	TimeReso κ_{org}[c]	Single κ_{org}[d]	Size-resolved κ_{BSOA}	Size-averaged κ_{BSOA}	Aged, Size-resolved κ_{BSOA}
0000–0200 JST	1	0.909	1.10	0.995	1	1.19	1.82
0200–0400 JST	1	0.926	1.04	1.01	1	1.17	1.83
0400–0600 JST	1	0.916	1.11	1.01	1	0.904	1.43
0600–0800 JST	1	0.868	1.05	0.950	1	5.58	9.00
0800–1000 JST	1	0.960	1.02	1.05	1	1.19	1.84
1000–1200 JST	1	1.10	1.05	1.19	1	1.14	1.68
1200–1400 JST	1	1.09	1.11	1.16	1	1.12	1.53
1400–1600 JST	1	1.14	1.14	1.21	1	1.12	1.52
1600–1800 JST	1	1.18	1.19	1.26	1	1.13	1.56
1800–2000 JST	1	1.06	1.13	1.15	1	1.15	1.62
2000–2200 JST	1	0.983	1.06	1.07	1	1.16	1.67
2200–0000 JST	1	0.948	1.04	1.04	1	1.18	1.82

[a] Time- and size-resolved κ_{org}.
[b] Time-averaged, size-resolved κ_{org}.
[c] Time-resolved, size-averaged κ_{org}.
[d] Time- and size-averaged κ_{org}.

Deleted: 913
Formatted ... [29]
Deleted: 09
Deleted: 3
Deleted: 81
Formatted ... [30]
Formatted ... [31]
Formatted ... [33]
Deleted: 3
Formatted ... [34]
Formatted ... [35]
Formatted ... [36]
Deleted: 84
Formatted Table ... [32]
Deleted: 920
Formatted ... [38]
Deleted: 10
Formatted ... [39]
Deleted: 00
Deleted: 899
Deleted: 42
Formatted ... [37]
Formatted ... [40]
Deleted: 7
Formatted ... [41]
Formatted ... [42]
Deleted: 04
Formatted ... [43]
Deleted: 1
Deleted: 3.61
Deleted: 5.82
Formatted ... [44]
Deleted: 4
Formatted ... [45]
Formatted ... [46]
Deleted: 04
Deleted: 82
Formatted ... [47]
Formatted ... [48]
Formatted ... [49]
Deleted: 18
Formatted ... [50]
Deleted: 08
Formatted ... [51]
Deleted: 10
Formatted ... [52]

Page 29: [1] Formatted dyg 2019/3/14 11:00:00

Normal

Page 29: [2] Formatted dyg 2019/3/14 11:00:00

Normal

Page 29: [3] Formatted Table dyg 2019/3/14 11:00:00

Formatted Table

Page 29: [4] Formatted dyg 2019/3/14 11:00:00

Normal, No widow/orphan control

Page 29: [5] Formatted dyg 2019/3/14 11:00:00

Normal

Page 29: [6] Formatted dyg 2019/3/14 11:00:00

Normal, No widow/orphan control

Page 29: [7] Formatted dyg 2019/3/14 11:00:00

Normal

Page 29: [8] Formatted dyg 2019/3/14 11:00:00

Normal, No widow/orphan control

Page 29: [9] Formatted dyg 2019/3/14 11:00:00

Normal

Page 29: [10] Formatted dyg 2019/3/14 11:00:00

Normal, No widow/orphan control

Page 29: [11] Formatted dyg 2019/3/14 11:00:00

Font: Calibri

Page 29: [12] Deleted dyg 2019/3/14 11:00:00

Page 29: [12] Deleted dyg 2019/3/14 11:00:00

Page 29: [13] Formatted dyg 2019/3/14 11:00:00

Normal

Page 29: [14] Formatted dyg 2019/3/14 11:00:00

Normal, No widow/orphan control

Page 29: [15] Formatted dyg 2019/3/14 11:00:00

Normal

Page 29: [16] Formatted dyg 2019/3/14 11:00:00

Normal, No widow/orphan control

Page 29: [17] Formatted dyg 2019/3/14 11:00:00

Normal

Page 29: [18] Formatted dyg 2019/3/14 11:00:00

Normal, No widow/orphan control

Page 29: [19] Formatted dyg 2019/3/14 11:00:00

Normal

Page 29: [20] Formatted dyg 2019/3/14 11:00:00

Normal, No widow/orphan control

Page 29: [21] Formatted dyg 2019/3/14 11:00:00

Normal

Page 29: [22] Formatted dyg 2019/3/14 11:00:00

Normal, No widow/orphan control

Page 29: [23] Formatted dyg 2019/3/14 11:00:00

Normal

Page 29: [24] Formatted dyg 2019/3/14 11:00:00

Normal, No widow/orphan control

Page 29: [25] Formatted dyg 2019/3/14 11:00:00

Normal

Page 29: [26] Formatted dyg 2019/3/14 11:00:00

Normal, No widow/orphan control

Page 29: [27] Formatted dyg 2019/3/14 11:00:00

Normal

Page 29: [28] Formatted dyg 2019/3/14 11:00:00

Normal, No widow/orphan control

Page 2: [29] Formatted dyg 2019/3/14 11:00:00

Font color: Auto

Page 2: [30] Formatted dyg 2019/3/14 11:00:00

Font color: Auto

Page 2: [31] Formatted dyg 2019/3/14 11:00:00

Font color: Auto

Page 2: [32] Formatted Table dyg 2019/3/14 11:00:00

Formatted Table

Page 2: [33] Formatted dyg 2019/3/14 11:00:00

Font color: Auto

Page 2: [34] Formatted dyg 2019/3/14 11:00:00

Font color: Auto

Page 2: [35] Formatted dyg 2019/3/14 11:00:00

Font color: Auto

Page 2: [36] Formatted dyg 2019/3/14 11:00:00

Font color: Auto

Page 2: [37] Formatted dyg 2019/3/14 11:00:00

Font color: Auto

Page 2: [38] Formatted dyg 2019/3/14 11:00:00

Font color: Auto

Page 2: [39] Formatted dyg 2019/3/14 11:00:00

Font color: Auto

Page 2: [40] Formatted	dyg	2019/3/14 11:00:00

Font color: Auto

Page 2: [41] Formatted	dyg	2019/3/14 11:00:00

Font color: Auto

Page 2: [42] Formatted	dyg	2019/3/14 11:00:00

Font color: Auto

Page 2: [43] Formatted	dyg	2019/3/14 11:00:00

Font color: Auto

Page 2: [44] Formatted	dyg	2019/3/14 11:00:00

Font color: Auto

Page 2: [45] Formatted	dyg	2019/3/14 11:00:00

Font color: Auto

Page 2: [46] Formatted	dyg	2019/3/14 11:00:00

Font color: Auto

Page 2: [47] Formatted	dyg	2019/3/14 11:00:00

Font color: Auto

Page 2: [48] Formatted	dyg	2019/3/14 11:00:00

Font color: Auto

Page 2: [49] Formatted	dyg	2019/3/14 11:00:00

Font color: Auto

Page 2: [50] Formatted	dyg	2019/3/14 11:00:00

Font color: Auto

Page 2: [51] Formatted	dyg	2019/3/14 11:00:00

Font color: Auto

Page 2: [52] Formatted	dyg	2019/3/14 11:00:00

Font color: Auto

Page 2: [53] Formatted	dyg	2019/3/14 11:00:00

Font color: Auto

Page 2: [54] Formatted dyg 2019/3/14 11:00:00

Font color: Auto

Page 2: [55] Formatted dyg 2019/3/14 11:00:00

Font color: Auto

Page 2: [56] Formatted dyg 2019/3/14 11:00:00

Font color: Auto

Page 2: [57] Formatted dyg 2019/3/14 11:00:00

Font color: Auto

Page 2: [58] Formatted dyg 2019/3/14 11:00:00

Font color: Auto

Page 2: [59] Formatted dyg 2019/3/14 11:00:00

Font color: Auto

Page 2: [60] Formatted dyg 2019/3/14 11:00:00

Font color: Auto

Page 2: [61] Formatted dyg 2019/3/14 11:00:00

Font color: Auto

Page 2: [62] Formatted dyg 2019/3/14 11:00:00

Font color: Auto

Page 2: [63] Formatted dyg 2019/3/14 11:00:00

Font color: Auto

Page 2: [64] Formatted dyg 2019/3/14 11:00:00

Font color: Auto

Page 2: [65] Formatted dyg 2019/3/14 11:00:00

Font color: Auto

Page 2: [66] Formatted dyg 2019/3/14 11:00:00

Font color: Auto

Page 2: [67] Formatted dyg 2019/3/14 11:00:00

Font color: Auto